Psat1-generated α-ketoglutarate and glutamine promote muscle stem cell activation and regeneration

Veronica Ciuffoli,[1] Xuesong Feng,[1] Kan Jiang,[2] Natalia Acevedo-Luna,[1] Kyung Dae Ko,[1] A. Hong Jun Wang,[1] Giulia Riparini,[1] Mamduh Khateb,[1] Brian Glancy,[3] Stefania Dell'Orso,[4] and Vittorio Sartorelli[1]

[1]Laboratory of Muscle Stem Cells and Gene Regulation, National Institute of Arthritis and Musculoskeletal and Skin Diseases, National Institutes of Health, Bethesda, Maryland 20892, USA; [2]Biodata Mining and Discovery Section, National Institute of Arthritis and Musculoskeletal and Skin Diseases, National Institutes of Health, Bethesda, Maryland 20892, USA; [3]Muscle Energetics, National Heart, Lung, and Blood Institute, National Institute of Arthritis and Musculoskeletal and Skin Diseases, National Institutes of Health, Bethesda, Maryland 20892, USA; [4]Genomic Technology Section, National Institute of Arthritis and Musculoskeletal and Skin Diseases, National Institutes of Health, Bethesda, Maryland 20892, USA

By satisfying bioenergetic demands, generating biomass, and providing metabolites serving as cofactors for chromatin modifiers, metabolism regulates adult stem cell biology. Here, we report that a branch of glycolysis, the serine biosynthesis pathway (SBP), is activated in regenerating muscle stem cells (MuSCs). Gene inactivation and metabolomics revealed that Psat1, one of the three SBP enzymes, controls MuSC activation and expansion of myogenic progenitors through production of the metabolite α-ketoglutarate (α-KG) and α-KG-generated glutamine. *Psat1* ablation resulted in defective expansion of MuSCs and impaired regeneration. Psat1, α-KG, and glutamine were reduced in MuSCs of old mice. α-KG or glutamine re-established appropriate muscle regeneration of adult conditional *Psat1*$^{-/-}$ mice and of old mice. These findings contribute insights into the metabolic role of Psat1 during muscle regeneration and suggest α-KG and glutamine as potential therapeutic interventions to ameliorate muscle regeneration during aging.

Adult stem cells sustain postnatal growth, maintain homeostasis, and ensure regeneration of tissues and organs in response to injury or disease. Muscle stem cells (MuSCs) reside in an anatomically and biochemically specialized niche (Yin et al. 2013; Relaix et al. 2021). Following injury, physical and biochemical modifications occurring in the niche cause MuSCs to leave quiescence (Kann et al. 2022; Ma et al. 2022). The ensuing MuSC division gives rise to a daughter stem cell returning to quiescence and one myogenic progenitor (MP; asymmetric division) or two MPs (symmetric division) that, after expansion, differentiate into myocytes, fusing with preexisting or new myofibers to repair damaged muscles (Kuang et al. 2007; Evano et al. 2020). The low energetic demands of quiescent MuSCs are supplied mainly by fatty acid oxidation (FAO) metabolism (Ryall et al. 2015b; Machado et al. 2017; Pala et al. 2018; Zeng et al. 2022). Consistently, FAO inhibition reduces MuSC colony formation and induces early MuSC differentiation (Cerletti et al. 2012; Pala et al. 2018). MuSC activation and MP proliferation are energetically costly processes required to sustain increased biosynthetic activity. In activated MuSCs and MPs, metabolic reprogramming from FAO to glycolysis generates ATP and pyruvate, which is subsequently used by mitochondria for oxidative phosphorylation (Rodgers et al. 2014; Ryall et al. 2015b; Baker et al. 2022; Hong et al. 2022; Sousa-Victor et al. 2022; Zeng et al. 2022). Besides providing ATP, glycolysis generates glycolytic intermediates required for the production of biomass and metabolites regulating chromatin modifiers (Ryall et al. 2015b; Das et al. 2017; Yucel et al. 2019). Genetic depletion of MuSCs induces features of age-associated dysfunctions, including impaired regeneration and loss of balance and coordination, suggesting that MuSCs play an important role in preserving muscle function during aging (Fry et al. 2015; Englund et al. 2020). Compromised regeneration observed in aging is indeed accompanied by impaired adult stem cell function. A plethora of cell-extrinsic and

-intrinsic factors contribute to the low regenerative capacity of aging MuSCs, including inflammation, extracellular matrix modifications, reduced heterogeneity, premature exit from quiescence, increased apoptosis, decreased cellular bioenergetics, and impaired proliferation (Brack et al. 2007; Bernet et al. 2014; Cosgrove et al. 2014; Almada and Wagers 2016; Baraibar et al. 2016; García-Prat et al. 2016; Feige et al. 2018; Liu et al. 2018; Lukjanenko et al. 2019; Palla et al. 2021; Dong et al. 2022; Sousa-Victor et al. 2022; Moiseeva et al. 2023; Shavlakadze et al. 2023).

In this study, we report that starting from the glycolytic intermediate metabolite 3-phosphoglycerate (3-PG), the serine biosynthesis pathway (SBP) is activated in regenerating MuSCs. Of the three SBP enzymes, Psat1 specifically regulates MuSC activation and expansion of MPs through production of the metabolite α-ketoglutarate (α-KG) and α-KG-generated glutamine. Genetic ablation of *Psat1* in MuSCs resulted in defective expansion of MuSCs and MPs, ultimately leading to muscle regenerative defects. Myogenic progenitors isolated from $Psat1^{-/-}$ mice displayed glycolytic defects, impaired proliferation, and reduced α-KG and glutamine levels. Glycolysis, myogenic proliferation, and muscle regeneration could be rescued in culture and in injured $Psat1^{-/-}$ mice by treatment with either α-KG or glutamine. We found that Psat1, α-KG, and glutamine levels were reduced in aged mice and that either α-KG or glutamine could improve mouse muscle regeneration and proliferation. These findings contribute mechanistic insights into the role of Psat1 as a generator of metabolites regulating MuSCs and MPs during muscle regeneration. They further identify α-KG and glutamine as potential therapeutic interventions to ameliorate muscle regeneration during aging.

Results

The serine biosynthesis pathway is induced in activated MuSCs and regenerating myogenic progenitors

The energetic and metabolic demands associated with MuSC activation and myogenic progenitor (MP) proliferation are sustained by both glycolysis and oxidative phosphorylation (Tang and Rando 2014; García-Prat et al. 2017; Pala et al. 2018; Yucel et al. 2019; Baker et al. 2022; Hong et al. 2022). Fatty acid oxidation (FAO) is prominent in quiescent MuSCs, and a glycolytic switch is observed in activated MuSCs and proliferating MPs (Ryall et al. 2015a, b; Machado et al. 2017; Zeng et al. 2022). In addition to generating lactate, pyruvate, and intermediate metabolites, glycolysis sustains amino acid synthesis (Stryer 1988). Starting from the glycolytic intermediate 3-phosphoglycerate (3-PG), the serine biosynthesis pathway (SBP) is consecutively regulated by three enzymes: phosphoglycerate dehydrogenase (Phgdh), phosphoserine aminotransferase (Psat1), and phosphoserine phosphatase (Psph) (Fig. 1A). Transcripts for these three enzymes were barely detected in freshly FACS-isolated MuSCs and became highly expressed in MuSCs cultured for 48 h (Fig. 1B–D; Ryall et al. 2015b). Moreover, single-cell RNA sequencing

(scRNA-seq) of uninjured or 60-h postinjury MuSCs revealed enrichment of Phgdh, Psat1, and Psph transcripts in activated 60-h postinjury MuSCs (Fig. 1E–H; Dell'Orso et al. 2019). The gene ontology terms "glycolytic process" and "L-serine biosynthetic/metabolic process" were enriched in data sets of both 60-h postinjury MuSCs and primary myoblasts (Fig. 1I,J; Dell'Orso et al. 2019). Thus, SBP is induced in activated MuSCs and MPs.

Psat1 regulates myoblast proliferation and α-KG synthesis

To initially evaluate their potential function, we reduced Phgdh, Psat1, or Psph by siRNA in primary myoblasts of adult (3- to 4-mo-old) mice and scored cell proliferation by 5-ethynyl-2′-deoxyuridine (EdU) incorporation assay. Impaired EdU incorporation was observed only in myoblasts receiving Psat1 siRNAs (Fig. 2A–C). Psat1 siRNAs reduced EdU incorporation also in human primary myoblasts or murine myogenic C2C12 cells (Supplemental Fig. S1A,B). Conversely, Psat1 overexpression increased EdU incorporation in C2C12 cells (Supplemental Fig. S1C). These results raise the question of how Psat1 and not the other two SBP enzymes influences myoblast proliferation. In addition to catalyzing the second step of serine biosynthesis, Psat1 promotes the synthesis of α-ketoglutarate (α-KG) from glutamate (Fig. 2D). To determine whether Psat1 regulates cell metabolites, we conducted untargeted metabolomics (see the Materials and Methods) (Fig. 2E). Aminomalonate, glycine, glucose-1-phosphate, and α-KG were significantly reduced in Psat1 siRNA transfected myoblasts (Fig. 2E; Supplemental Table S1). Reduced α-KG in Psat1 siRNA myoblasts was confirmed with an independent assay (Fig. 2F). Instead, the SBP-related amino acids serine, methionine, glutamic acid, cysteine, and alanine were not modified in Psat1 siRNA transfected myoblasts (Supplemental Fig. S1D; Supplemental Table S1).

Psat1 is required for muscle regeneration

Whole-body *Psat1* knockout mice present growth retardation, exencephaly, and craniofacial abnormalities at E14.5 (White et al. 2013). Thus, to ablate *Psat1* in MuSCs, we generated $Psat1^{fl/fl}$ mice by introducing *loxP* sites flanking the second exon of *Psat1* and crossed the resulting mice with either constitutive $Pax7^{Cre}$ or tamoxifen-inducible (TMX) $Pax7^{CreERT2}$ to generate constitutive $Pax7^{Cre}$; $Psat1^{fl/fl}$ ($Psat1^{cKO}$) and inducible $Pax7^{CreERT2};Psat1^{fl/fl}$ ($Psat1^{iKO}$) mice, respectively. $Psat1^{cKO}$ mice were born at the expected Mendelian ratios and did not display overt muscle abnormalities, indicating a dispensable role of Psat1 in MuSCs during development (Supplemental Fig. S2A–F). We investigated the role of Psat1 during muscle regeneration in $Psat1^{iKO}$ mice. TMX treatment for five consecutive days resulted in (1) ~75% deletion of *Psat1* exon2, (2) reduced Psat1 exon2 transcripts, and (3) decreased Psat1 protein in $Psat1^{iKO}$ 3-d postinjury (dpi) MuSCs (Fig. 3A–C). After TMX treatment, muscle injury was induced with notexin, and regeneration was evaluated
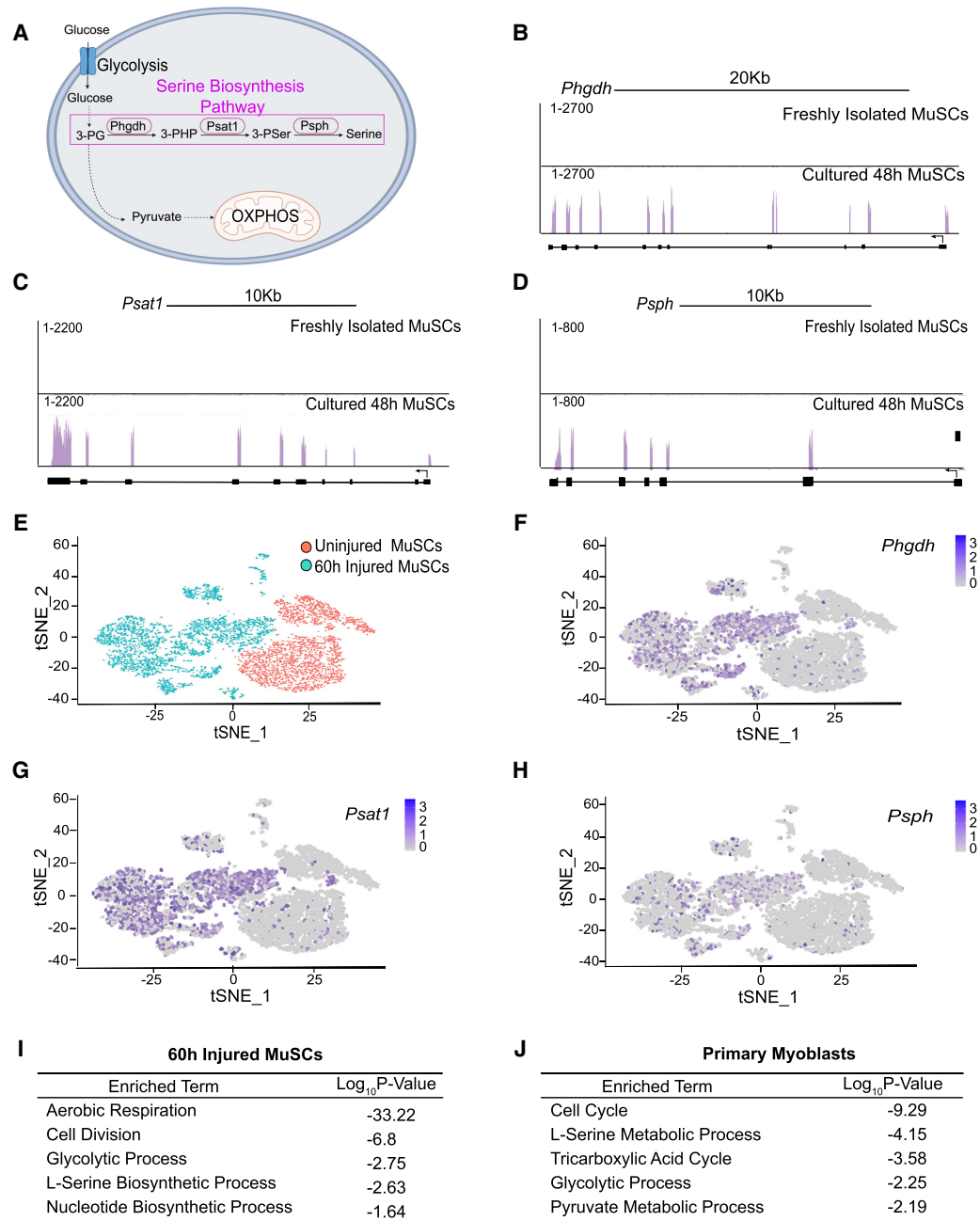
Figure 1. The serine biosynthesis pathway is activated in injured MuSCs. (*A*) Schematic representation of the serine biosynthesis pathway. (3-PG) 3-phosphoglycerate, (Phgdh) phosphoglycerate dehydrogenase, (Psat1) phosphoserine aminotransferase, (Psph) phosphoserine phosphatase. (*B–D*) RNA-seq tracks of Phgdh, Psat1, and Psph transcripts from freshly FACS-isolated and 48-h cultured MuSCs. (*E*) scRNA-seq graph-based clustering of freshly FACS-isolated MuSCs from uninjured or 60-h injured muscles. (*F–H*) Expression pattern of Phgdh, Psat1, and Psph transcripts from scRNA-seq data sets obtained from uninjured or 60-h injured MuSCs. Data were generated using a custom script (https://zenodo.org/records/10211509). (*I,J*) Gene ontology of selected terms enriched in 60-h injured MuSCs (*I*) and cultured primary myoblasts (*J*).

at 3, 7, and 28 dpi (Fig. 3D). These three time points were chosen because they coincide with MuSC proliferation, myocyte differentiation, and MuSCs returning to quiescence. To ease identification, MuSCs were lineage-traced by crossing $Psat1^{iKO}$ with $ROSA26^{STOP-Sun1-GFP}$ mice ($Psat1^{iKO\ nGFP}$) (Supplemental Fig. S2G). In vivo cell prolif-

eration at 3 dpi was monitored by intraperitoneal (IP) EdU injection. The percentage of MuSCs incorporating EdU was significantly lower in 3-dpi $Psat1^{iKO\ nGFP}$ mice compared with littermate control ($Pax7^{CreERT2};Psat1^{+/+nGFP}$) mice (Fig. 3E). The percentage of Pax7^{+}, MyoD[+], and Myogenin^{+} cells was decreased at 7 dpi (Fig. 3F). Finally, Pax7^{+}
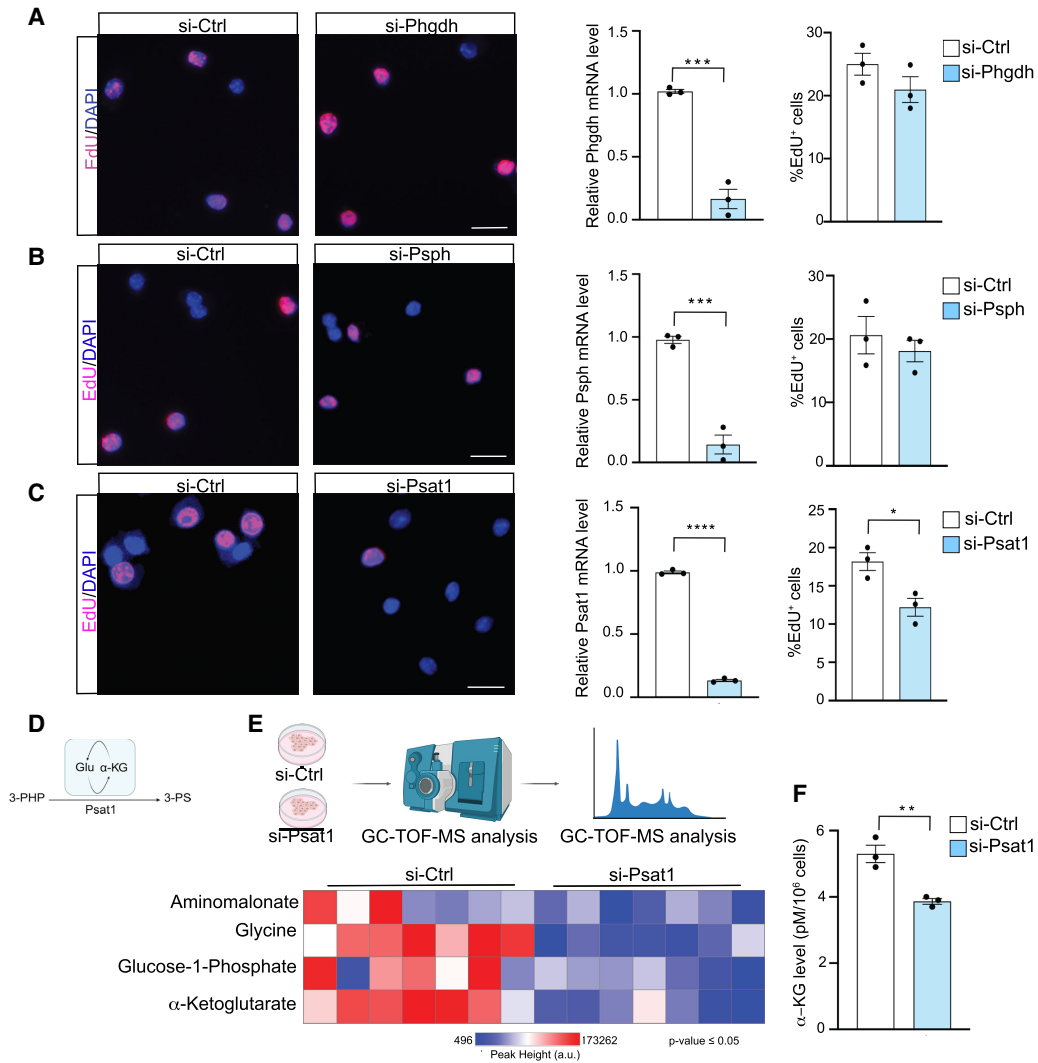
Figure 2. Psat1 regulates proliferation of primary myoblasts (*A–C, left* panels) Representative images of EdU incorporation in primary mouse myoblasts transfected with control (Ctrl), Phgdh (*A*), Psph (*B*), or Psat1 (*C*) siRNA. Scale bar, 20 μm. (*Right* panels) Data represent mean ± SEM; *n* = 3. (*) $P \leq 0.05$, (***) $P \leq 0.001$, (****) $P \leq 0.0001$. (*D*) Schematic representation of Psat1-mediated α-KG production. (3-PHP) 3-phosphohydroxypyruvate, (3-PS) 3-phosphoserine, (Glu) glutamate. (*E*) Schematic of GC-TOF-MS (*top* panel) and heat map (*bottom* panel) based on peak height (arbitrary units [a.u.]) of metabolites identified by GC-TOF-MS in si-Ctrl or si-Psat1 primary myoblasts. Each row represents a metabolite, and each column represents a sample. *n* = 7. (*F*) α-KG levels in si-Ctrl or si-Psat1 primary mouse myoblasts. Data represent mean ± SEM; *n* = 3. (**) $P \leq 0.01$.

cells returning to a niche position and muscle cross-sectional area (CSA) were reduced in 28-dpi *Psat1*[iKO] mice compared with littermate control mice (Fig. 3G,H). Apoptosis was not increased in *Psat1*[iKO] mice (Supplemental Fig. S2H), and no differences were observed in the number of cells positive for the senescence-associated marker p16[Ink4a] in control and *Psat1*[iKO] mice (Supplemental Fig. S2I).

α-KG improves glycolysis, promotes glutamine synthesis, and restores proliferation of Psat1^{−/−} *myoblasts*

In agreement with the results observed in myoblasts receiving Psat1 siRNA (Fig. 2), myoblasts isolated from

Psat1[cKO] mice have reduced proliferation compared with those of control littermate mice (Fig. 4A), and RNA-seq performed on FACS-isolated 3-dpi *Psat1*[iKO] MuSCs revealed down-regulation of genes involved in skeletal muscle tissue development and up-regulation of genes preventing cell growth (negative regulation of cell growth) (Supplemental Fig. S3A; Supplemental Table S2). α-KG regulates the activity of α-KG-dependent dioxygenases, including histone H3K27 and H3K9 demethylases and the TET family of DNA demethylases (Klose and Zhang 2007; Carey et al. 2015; Islam et al. 2018). Because of decreased α-KG levels observed in *Psat1*[cKO] myoblasts (Supplemental Fig. S3B), we set out to investigate whether histone H3K27me3 and H3K9me3 and
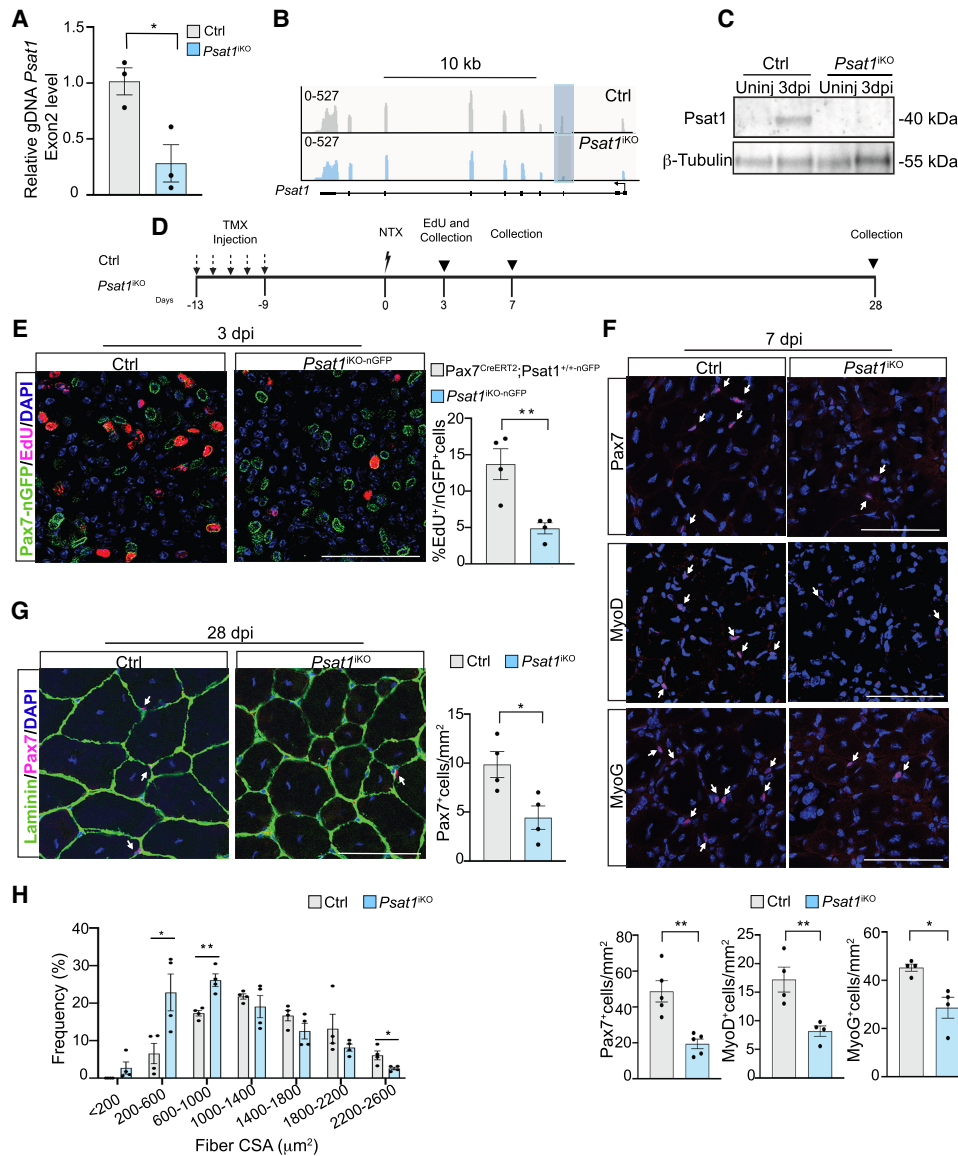
Figure 3. Psat1 is required for muscle regeneration. (*A*) Quantitative PCR of genomic DNA from MuSCs of control or *Psat1*[iKO] mice. The amplified region corresponds to Psat1 exon2. Data represent mean ± SEM; $n = 3$. (*) $P \leq 0.05$. (*B*) RNA-seq tracks documenting reduced exon2 transcripts (boxed area) in *Psat1*[iKO] 3-dpi MuSCs. (*C*) Immunoblot for Psat1 from uninjured (Uninj) or 3-dpi MuSCs from control or *Psat1*[iKO] mice. β-Tubulin served as the loading control. (*D, left* panels) Scheme indicating tamoxifen (TMX) treatment and the notexin (NTX)-induced muscle injury regimen. (*E*) Representative images of muscle sections of 3-dpi littermate control (*Pax7*[CreERT2];*Psat1*[+/+nGFP]) or *Psat1*[iKO nGFP] mice intraperitoneally injected with 100 μL of 40 mM EdU solution. GFP identifies MuSCs and DAPI cell nuclei. Scale bar, 75 μm. (*Right* panel) Quantification is shown as percentage of EdU⁺/GFP⁺ cells over total number of GFP⁺ cells. Data represent mean ± SEM; $n = 4$. (**) $P \leq 0.01$. (*F, top* panels) Pax7, MyoD, and MyoG immunostaining of TA/EDL muscle sections from control or *Psat1*[iKO] 7-dpi mice. Scale bar, 75 μm. (*Bottom* panels) Quantification of Pax7⁺, MyoD⁺, and MyoG⁺ cells in control or *Psat1*[iKO] muscle sections. Data represent mean ± SEM, $n = 4$–5. (*) $P \leq 0.05$, (**) $P \leq 0.01$. (*G, left* panels) Pax7 and laminin immunostaining of 28-dpi control or *Psat1*[iKO] muscle sections. Scale bar, 75 μm. (*Right* panel) Quantification of Pax7⁺ cells in control or *Psat1*[iKO] muscle sections. Data represent mean ± SEM; $n = 4$. (*) $P \leq 0.05$. (*H*) Percentage size groups of the fiber cross-sectional area from 28-dpi control or *Psat1*[iKO] mice. Data represent mean ± SEM; $n = 4$. (*) $P \leq 0.05$, (**) $P \leq 0.01$.

demethylated 5′-hydroxymethylcytosine (5hmC) marks were modified. Total H3K27me3 and H3K9me3 levels were comparable in control and *Psat1*[cKO] primary myoblasts and were not modified by α-KG (Supplemental Fig. S3C–F). We performed H3K27me3 CUT&RUN and 5hmC immunoprecipitation sequencing (5hmC-seq) as-

says in control and *Psat1*[cKO] myoblasts and interrogated H3K27me3 and 5hmC at genes down-regulated or up-regulated in *Psat1*[cKO] myoblasts. Integrated analysis of these data sets did not reveal significant H3K27me3 or 5hmC modifications occurring at differentially regulated genes in *Psat1*[cKO] myoblasts (Supplemental Fig. S3G–L;

Supplemental Table S3). We conclude that it is unlikely that reduced α-KG levels have functional consequences by affecting H3K27me3, H3K9me3, or 5hmC epigenetic marks in *Psat1*^{cKO} myoblasts. We then asked whether α-KG had any discernable effect on myoblast proliferation. Adding 1 mM cell-permeable dimethyl-α-KG (DM-αKG) to the culture medium at 24 h (Hwang et al. 2016) improved EdU incorporation in *Psat1*^{cKO} myoblasts (Fig. 4B). α-KG is generated in the mitochondria and cytosol by isocitrate dehydrogenase (IDH) and by Psat1 during the glycolysis-branched serine biosynthesis pathway, serving as a precursor of glutamine (Locasale and Cantley 2011). Psat1 also regulates de novo biosynthesis of serine that further feeds into one-carbon metabolism, comprising the folate and methionine cycles (Stryer 1988). We reasoned that if the reduced α-KG levels observed in *Psat1*^{cKO} myoblasts were affecting the tricarboxylic acid (TCA) cycle, providing downstream succinate would rescue myoblast proliferation (Fig. 4B, scheme). Surprisingly, while α-KG improved *Psat1*^{cKO} myoblast proliferation, succinate did not (Fig. 4B), suggesting that α-KG does not exert its effects on *Psat1*^{cKO} myoblasts through the mitochondrial TCA cycle. In agreement with these initial observations, total mitochondrial content (determined by MitoTracker Green) and energetic activity (expressed as MitoTracker Red/MitoTracker Green ratio intensity) were not modified in *Psat1*^{cKO} myoblasts compared with control myoblasts (Supplemental Fig. S4A). Basal, maximal, and spare mitochondrial respiratory capacities were also comparable in control and *Psat1*^{cKO} myoblasts, and α-KG did not modify them (Fig. 4C). In contrast, total glycolysis, glycolytic capacity, and glycolytic reserve were decreased in *Psat1*^{cKO} myoblasts and were corrected by α-KG (Fig. 4D). Consistently, α-KG increased glycolysis-generated ATP (glycoATP) in *Psat1*^{cKO} myoblasts (Supplemental Fig. S4B). α-KG can be converted to intermediate glutamate (Glu) and further amidated to glutamine (Gln) by glutamine synthetase (GS) (Fig. 4E). Glutamate levels were decreased in *Psat1*^{cKO} myoblasts, and α-KG increased them (Supplemental Fig. S4C). Glutamine was also decreased in *Psat1*^{cKO} myoblasts, and α-KG corrected glutamine levels (Fig. 4F). Moreover, glutamine could improve *Psat1*^{cKO} myoblast proliferation (Fig. 4G). Glutamine also increased glycoATP production (Supplemental Fig. S4D). To evaluate whether α-KG exerts its effects through glutamine, we inhibited GS activity with the GS competitive inhibitor methionine sulfoximine (MSO) (Fig. 4E; Krajewski et al. 2008) and measured *Psat1*^{cKO} myoblast proliferation without or with α-KG supplementation. While α-KG could restore proliferation, GS inhibition prevented α-KG-mediated improved proliferation of *Psat1*^{cKO} myoblasts (Fig. 4H, MSO + DM-α-KG panel). The inhibitory effects of MSO on α-KG-treated *Psat1*^{cKO} myoblast proliferation were rescued by supplementing the culture medium with excess glutamine (Fig. 4H, MSO + Gln panel). The effects of α-KG, glutamine, and MSO observed on *Psat1*^{cKO} myoblast proliferation were paralleled by concordant patterns of glycolysis and glycolytic capacity (Supplemental Fig. S4E). Glycolytic capacity (an indication of glycolytic efficacy when mito-chondrial activity is inhibited by oligomycin) was improved by α-KG also in MSO-treated *Psat1*^{cKO} myoblasts, suggesting potential metabolic compensation that is, however, insufficient to rescue proliferation (Fig. 4H). Glycine, which was reduced in Psat1 siRNA myoblasts (Fig. 2E), is required for MuSC and MP function (Gheller et al. 2021). In agreement with these findings, supplementing *Psat1*^{cKO} myoblasts with glycine increased EdU incorporation (Supplemental Fig. S4F) and improved glycolysis (Supplemental Fig. S4G). On the other hand, supplementation with the serine biosynthesis-derived one-carbon metabolite S-adenosyl methionine (SAM) or folic acid (FA) had no effect on *Psat1*^{cKO} myoblast proliferation (Supplemental Fig. S4H,I). Overall, the results of these experiments indicate that α-KG improves glycolysis and that α-KG and its derivative glutamine improve *Psat1*^{cKO} myoblast proliferation, while succinate, FA, and SAM do not.

α-KG or glutamine rescues impaired muscle regeneration in Psat1^{iKO} mice

We next tested whether α-KG may also correct defective muscle regeneration observed in *Psat1*^{iKO} mice. Control and *Psat1*^{iKO} mice were treated with TMX for five consecutive days followed by a 7-d washout period. One day before notexin injection (day −1), mice were intraperitoneally injected with either vehicle (PBS) or 600 mg/kg α-KG (Tran et al. 2020). IP α-KG injections were repeated 1, 3, and 5 d after notexin injection (Fig. 5A). Since our experiments indicated an effect of Psat1 on MP proliferation (which peaks at 3 dpi), we reasoned that IP α-KG injections beyond 5 dpi may not be necessary. MuSC proliferation was monitored by IP EdU injection 1 h before sample collection at 3 dpi. Muscle samples were collected at 3 dpi to assess proliferation and at 28 dpi to determine muscle regeneration. At 3 dpi, α-KG improved EdU incorporation in MuSCs of *Psat1*^{iKO} mice (Fig. 5B). At 28 dpi, α-KG-treated *Psat1*^{iKO} mice displayed an increased number of MuSCs located in a niche position to levels comparable with those observed in control mice (Fig. 5C). The muscle cross-sectional area (CSA) of *Psat1*^{iKO} mice was also increased by α-KG (Fig. 5D). Next, we tested whether glutamine could also improve EdU incorporation in MuSCs of *Psat1*^{iKO} mice. Muscle samples of injured *Psat1*^{iKO} mice receiving IP injections of 500 mg/kg glutamine collected at 3 dpi revealed increased EdU incorporation in MuSCs compared with control (*Pax7*^{CreERT2}; *Psat1*^{+/+nGFP}) mice (Supplemental Fig. S5). Thus, α-KG and glutamine not only improve proliferation of cultured *Psat1*^{cKO} myoblasts, they also ameliorate MuSC proliferation and muscle regeneration of *Psat1*^{iKO} mice.

α-KG or glutamine increases proliferation of aging mouse myoblasts

The number and regenerative potential of MuSCs are reduced during aging (Conboy et al. 2003; Carlson et al. 2009; Chakkalakal et al. 2012; Sousa-Victor et al. 2022). We investigated expression of Psat1 in 3-dpi MuSCs of
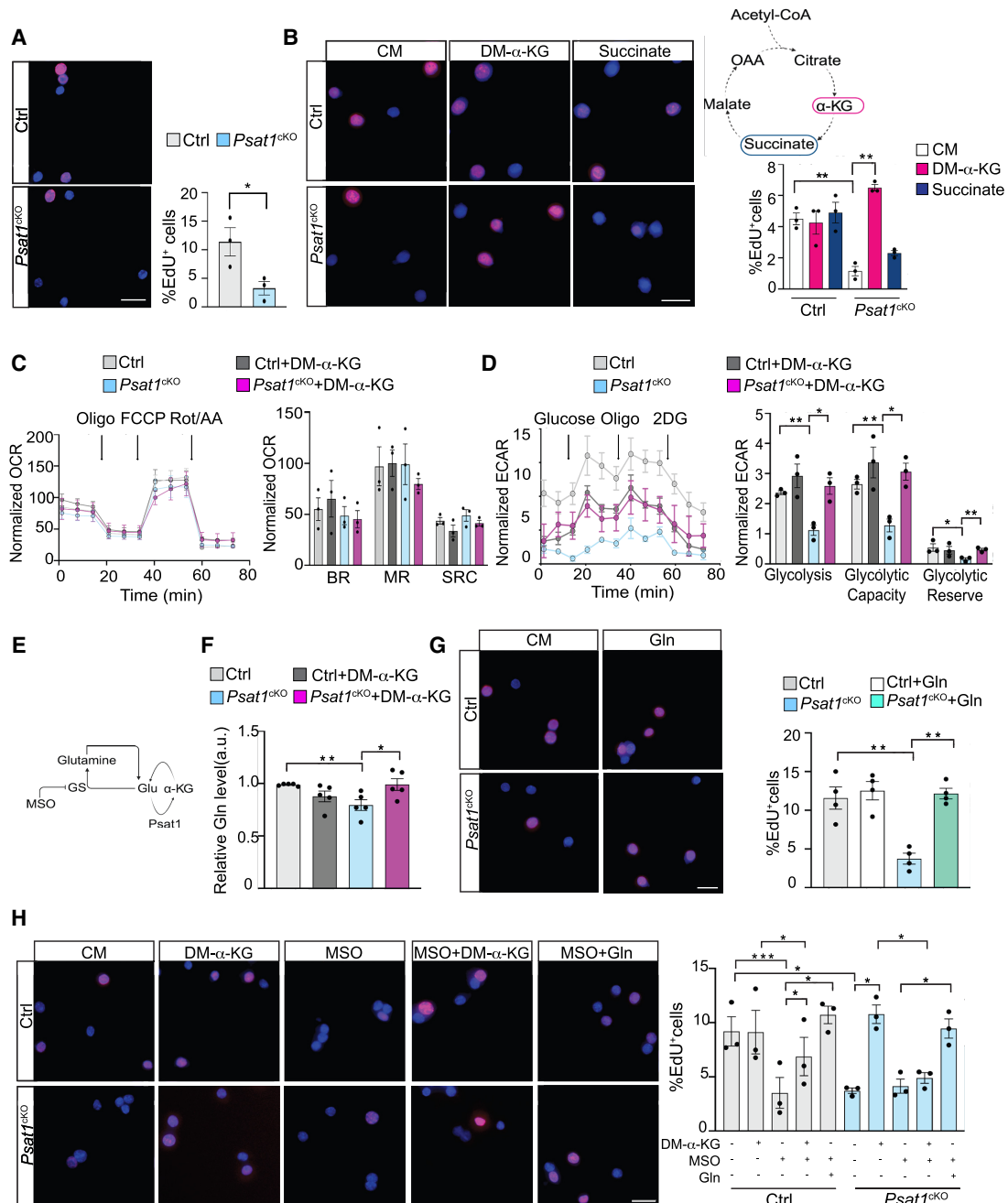
Figure 4. α-KG or glutamine rescues *Psat1*[cKO] myoblast proliferation. (*A, left* panels) Representative images of EdU incorporation in control (Ctrl) or *Psat1*[cKO] myoblasts. Scale bar, 20 μm. (*Right* panel) Data represent mean ± SEM; *n* = 3. (*) $P \leq 0.05$. (*B, left* panels) Control or *Psat1*[cKO] myoblasts were cultured in control medium (CM) or medium supplemented with 1 mM DM-α-KG or 1 mM succinate for 24 h and pulsed with 10 μM EdU for 2 h before cell processing. Scale bar, 20 μm. (*Right* panel) Schematic representation of the tricarboxylic acid cycle. Data represent mean ± SEM; *n* = 3. (**) $P \leq 0.01$. (*C*) Normalized oxygen consumption rates (OCRs) of control or *Psat1*[cKO] myoblasts in CM or medium supplemented with 1 mM DM-α-KG. Data represent mean ± SEM; *n* = 3. (BR) Basal respiration, (MR) maximal respiration, (SRC) spare respiratory capacity. (*D*) Normalized extracellular acidification rate (ECAR) of control or *Psat1*[cKO] myoblasts in CM or medium supplemented with 1 mM DM-α-KG. Data represent mean ± SEM; *n* = 3. (*) $P \leq 0.05$, (**) $P \leq 0.01$. (*E*) Schematic representation of the glutamine–glutamate–α-KG metabolism. (Glu) Glutamate, (GS) glutamine synthetase. (MSO) methionine sulfoximide. (*F*) Glutamine (Gln) measurements in control or *Psat1*[cKO] myoblasts cultured in CM or treated with 1 mM DM-α-KG for 24 h. Data represent mean ± SEM; *n* = 5. (*) $P \leq 0.05$, (**) $P \leq 0.01$. (*G, left* panels) Control or *Psat1*[cKO] myoblasts were cultured in CM or medium supplemented with 4 mM glutamine (Gln) for 24 h and exposed to 10 μM EdU for 2 h before cell processing. Scale bar, 20 μm. (*Right* panel) Data represent mean ± SEM; *n* = 4. (**) $P \leq 0.01$. (*H, left* panels) Control or *Psat1*[cKO] myoblasts were cultured in CM or medium supplemented with 1 mM DM-α-KG, 4 mM glutamine (Gln), 1 mM MSO, MSO + DM-α-KG, or MSO + glutamine for 24 h and exposed to 10 μM EdU for 2 h before cell processing. Scale bar, 20 μm. (*Right* panel) Data represent mean ± SEM; *n* = 3. (*) $P \leq 0.05$, (***) $P \leq 0.001$.
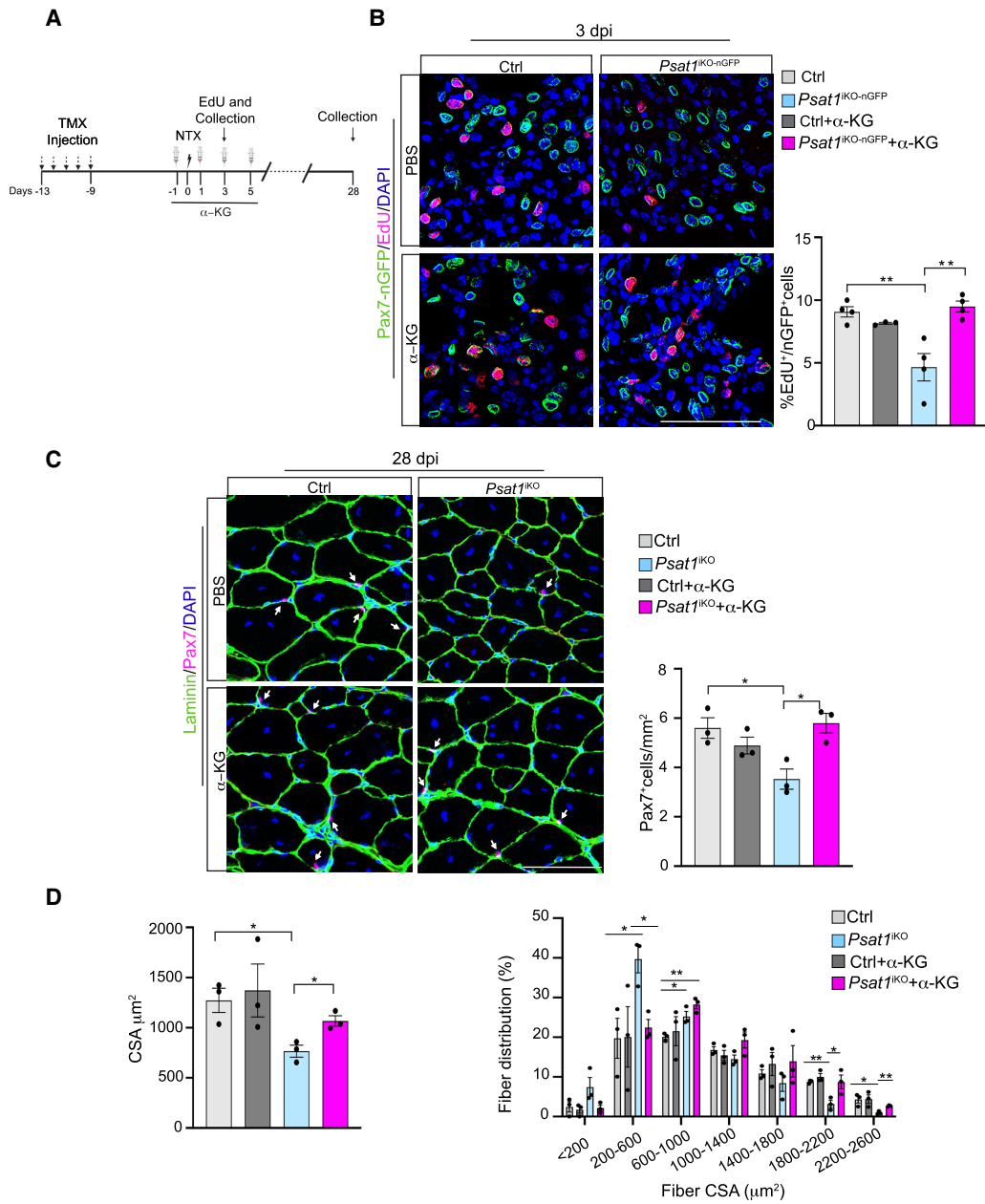
A

B

C

D

Figure 5. α-KG rescues impaired muscle regeneration in *Psat1*[iKO] mice. (*A*) Schematic representation of tamoxifen (TMX)- or notexin (NTX)-induced muscle injury and α-KG treatment in control or *Psat1*[iKO] mice. (*B*, *left* panels) Representative images of muscle sections of 3-dpi littermate control (*Pax7*[CreERT2];*Psat1*[+/+nGFP]) or *Psat1*[iKO nGFP] mice intraperitoneally injected with PBS or 600 mg/kg α-KG. One hour before harvesting, mice were intraperitoneally injected with 100 µL of 40 mM EdU solution. GFP identifies MuSC and DAPI cell nuclei. Scale bar, 75 µm. (*Right* panel) Quantification of the percentage of EdU$^+$/GFP$^+$ cells over total number of GFP$^+$ cells. Data represent mean ± SEM; $n = 3-4$. (**) $P \leq 0.01$. (*C*, *left* panels) Representative muscle sections showing Pax7 and laminin immunostaining of 28-dpi control (*Pax7*^{+/+};*Psat1*^{fl/fl}) or *Psat1*[iKO] mice treated with PBS or 600 mg/kg α-KG. Scale bar, 75 µm. (*Right* panel) Quantification of Pax7$^+$ cells in control or *Psat1*[iKO] muscle sections. Data represent mean ± SEM; $n = 3$. (*) $P \leq 0.05$. (*D*) Muscle fiber cross-sectional area (CSA) quantification (*left* panel) and percentage of size groups (*right* panel) of 28-dpi muscle sections in control or *Psat1*[iKO] mice treated with PBS or 600 mg/kg α-KG. Data represent mean ± SEM; $n = 3$. (*) $P \leq 0.05$, (**) $P \leq 0.01$.

old (23- to 24-mo-old) mice and found it to be reduced compared with that of adult (3- to 4-mo-old) 3-dpi MuSCs (Fig. 6A,B). Moreover, α-KG levels were diminished in primary myoblasts of old (Fig. 6C) or geriatric (31- to 32-mo-old) (Supplemental Fig. S6A) mice compared with those of

adult mice. These commonalities between *Psat1*[cKO] and myoblasts of aging mice prompted us to investigate their metabolic profiles. As observed for *Psat1*[cKO] myoblasts (Fig. 4D), myoblasts of geriatric mice displayed reduced glycolysis (Supplemental Fig. S6B). In addition, and in
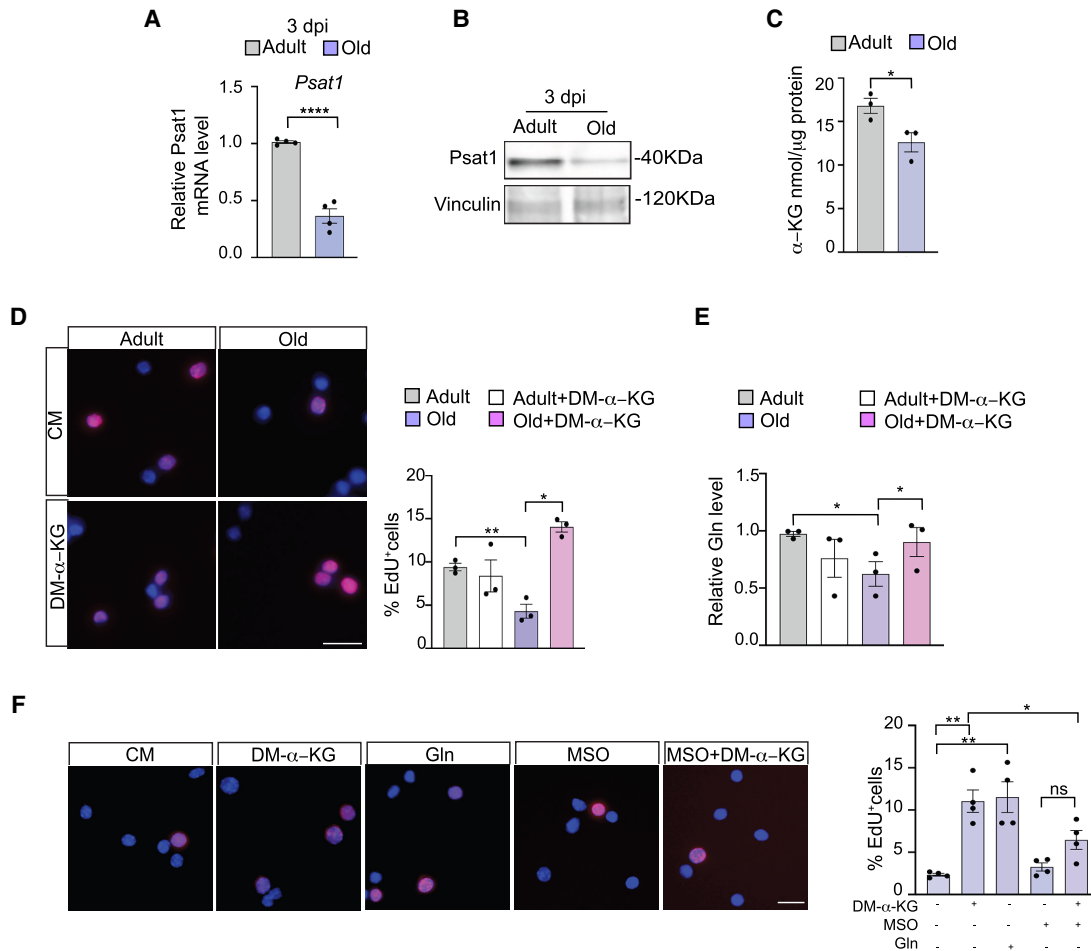
Figure 6. α-KG increases proliferation of myoblasts from aging mice. (*A*) RT-qPCR of Psat1 mRNA level in 3-dpi MuSCs isolated from adult (3-mo-old) or old (24-mo-old) mice. Data represent mean ± SEM of FC relative to Psat1 transcript level in adults. 18S transcripts were used as housekeeping control; $n = 4$. (****) $P \leq 0.0001$. (*B*) Immunoblot of Psat1 protein in 3-dpi MuSCs from adult or old mice. Vinculin served as the loading control. (*C*) α-KG levels in primary myoblasts of adult and old mice. Data represent mean ± SEM; $n = 3$. (*) $P \leq 0.05$. (*D, left* panel) Representative immunofluorescence images of EdU incorporation in primary myoblasts of adult or old mice cultured in control medium (CM) or treated with 1 mM DM-α-KG for 24 h. DAPI identifies cell nuclei. Scale bar, 20 μm. (*Right* panel) Quantification of the percentage of EdU⁺ cells over total number of nuclei. Data represent mean ± SEM; $n = 3$. (*) $P \leq 0.05$, (**) $P \leq 0.01$. (*E*) Glutamine (Gln) levels in myoblasts of adult or old mice cultured in control medium or treated with 1 mM DM-α-KG for 24 h. Data represent mean ± SEM; $n = 3$. (*) $P \leq 0.05$. (*F, left* panel) Myoblasts of old mice were cultured in control medium (CM) or in the presence of 1 mM DM-α-KG, 4 mM glutamine (Gln), 1 mM MSO, or 1 mM MSO + 1 mM DM-α-KG for 24 h and exposed to 10 μM EdU for 2 h before cell processing. Scale bar, 20 μm. (*Right* panel) Data represent mean ± SEM; $n = 3$–4. (*) $P \leq 0.05$, (**) $P \leq 0.01$.

agreement with previous findings (Baker et al. 2022; Hong et al. 2022), geriatric myoblasts also had decreased mitochondrial respiration (Supplemental Fig. S6C). DM-α-KG (1 mM for 24 h) did not improve mitochondrial respiration but ameliorated glycolysis of geriatric myoblasts (Supplemental Fig. S6B,C). Furthermore, DM-α-KG increased EdU incorporation in myoblasts of both old and geriatric mice to levels comparable with those observed in adult myoblasts (Fig. 6D; Supplemental Fig. S6D). Supplementing myoblasts of old mice with DM-α-KG increased intracellular glutamine (Fig. 6E). Proliferation of old myoblasts was also improved by glutamine, and the proproliferative effects of α-KG on myoblasts of old mice were blunted by GS inhibition (Fig. 6F). Thus, even though mitochondrial respiration was not corrected, proliferation of myoblasts from old mice was improved by α-KG or glutamine.

Age-related decline of muscle regeneration is improved by exogenously supplied α-KG or glutamine

We tested whether, beside promoting cell proliferation of cultured aged myoblasts, α-KG may also improve muscle regeneration of aging mice. To this end, 23- to 24-mo-old mice were intraperitoneally injected with either vehicle (PBS) or 600 mg/kg α-KG 1 d before injury (day −1) and 1, 3, and 5 dpi (Fig. 7A), and Pax7⁺ cells and CSA were evaluated at 15 and 28 dpi. At both time points, mice receiving α-KG displayed a significant increase in the number of
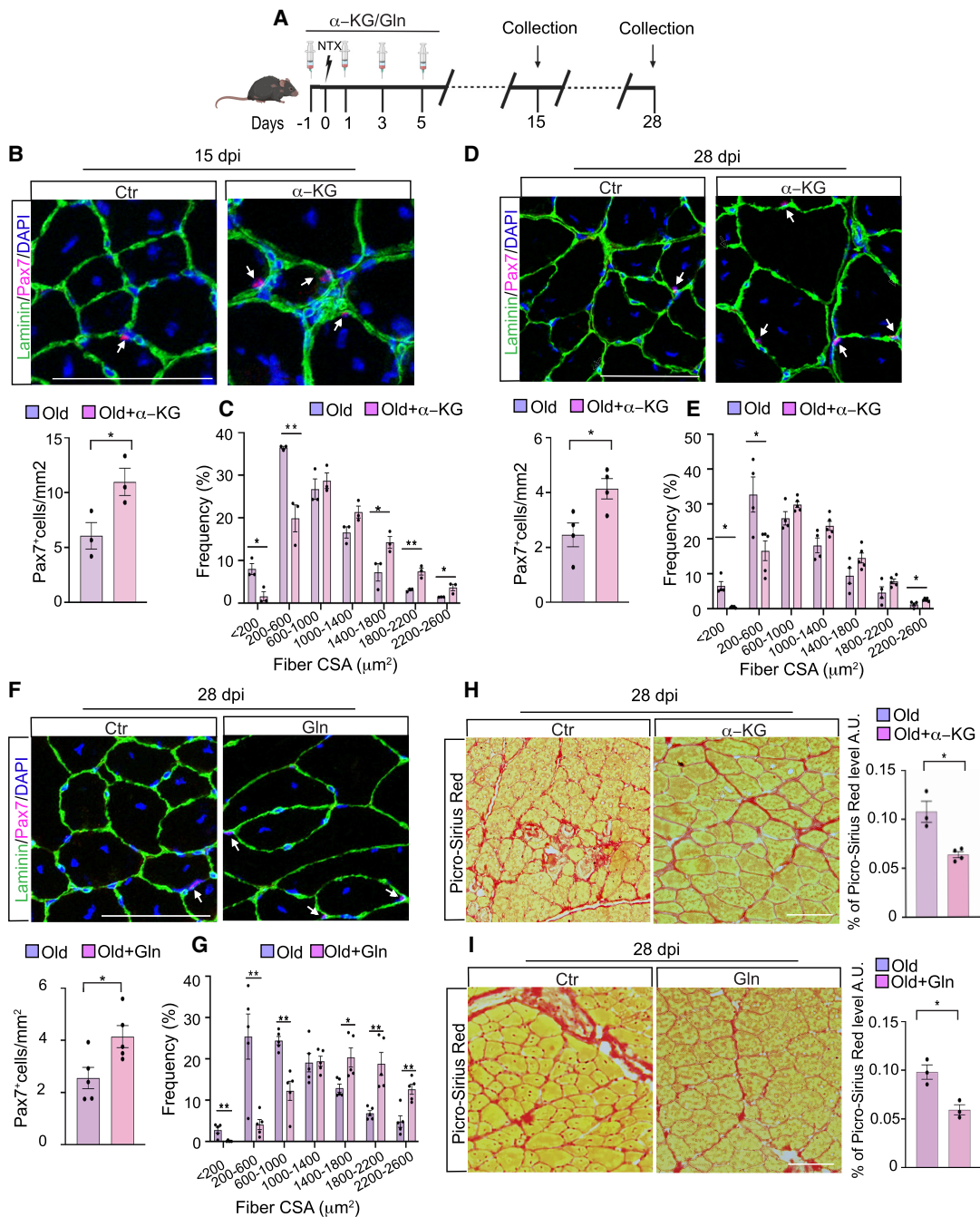
Figure 7. α-KG or glutamine improves muscle regeneration of old mice. (*A*) Schematic representation of notexin and α-KG or glutamine (α-KG/Gln) treatment in old mice. (*B, top* panels) Representative images of muscle sections of 15-dpi old (23- to 24-mo-old) mice intraperitoneally injected with either PBS or 600 mg/kg α-KG and immunostained with Pax7 antibody. Scale bar, 75 μm. (*Bottom* panel) Quantification of Pax7⁺ cells in PBS- or α-KG-treated mice. Data represent mean ± SEM; $n = 3$. (*) $P \leq 0.05$. (*C*) Percentage size group of fiber cross-sectional area from 15-dpi old (23- to 24-mo-old) mice intraperitoneally injected with either PBS or α-KG. Data represent mean ± SEM; $n = 3$. (*) $P \leq 0.05$, (**) $P \leq 0.01$. (*D,E*) Experimental conditions and measurements are as described in *B* and *C*, except that mice were evaluated at 28 dpi. $n = 4$–5. (*F, top* panels) Representative images of muscle sections of 28-dpi old (23- to 24-mo-old) mice intraperitoneally injected with either PBS or 500 mg/kg glutamine (Gln) and immunostained with Pax7 antibody. Scale bar, 75 μm. (*Bottom* panel) Quantification of Pax7⁺ cells in PBS- or glutamine-treated mice. Data represent mean ± SEM; $n = 5$. (*) $P \leq 0.05$. (*G*) Percentage size group of fiber cross-sectional area from 28-dpi old (23- to 24-mo-old) mice intraperitoneally injected with either PBS or glutamine (Gln). Data represent mean ± SEM; $n = 5$. (*) $P \leq 0.05$, (**) $P \leq 0.01$. (*H, left* panels) Representative images of muscle sections of 28-dpi old (23- to 24-mo-old) mice intraperitoneally injected with either PBS or α-KG and stained with Picro-Sirius red. Scale bar, 75 μm. (*Right* panel) Quantification of Picro-Sirius red staining in PBS- or α-KG-treated mice. Data represent mean ± SEM; $n = 3$–4. (*) $P \leq 0.05$. (*I, left* panels) Representative images of muscle sections of 28-dpi old (23- to 24-mo-old) mice intraperitoneally injected with either PBS or glutamine (Gln) and stained with Picro-Sirius red. Scale bar, 75 μm. (*Right* panel) Quantification of Picro-Sirius red staining in PBS- or glutamine-treated mice. Data represent mean ± SEM; $n = 3$. (*) $P \leq 0.05$.

Pax7^{+} cells and CSA (Fig. 7B–E). At 28 dpi, α-KG treatment resulted also in decreased fibrosis (Fig. 7F–H). We further investigated the effects of glutamine. Mice (23–24 mo old) were intraperitoneally injected with either vehicle (PBS) or 500 mg/kg glutamine 1 d before injury (day −1) and 1, 3, and 5 dpi, and the number of Pax7^{+} cells, CSA, and fibrosis were evaluated at 28 dpi. As observed with α-KG, glutamine also improved muscle regeneration, as determined by the increased number of Pax7^{+} cells and CSA and reduced fibrosis (Fig. 7F,G,I).

Discussion

Activation of T lymphocytes, dendritic cells, and MuSCs is accompanied by glycolytic reprogramming (Jones and Thompson 2007; Krawczyk et al. 2010; Ryall et al. 2015b). Glycolysis is indispensable for retinal progenitor proliferation and biosynthesis (even when it is not used for ATP production) (Agathocleous et al. 2012) and for lung alveolar stem cell differentiation (Wang et al. 2023). Moreover, a metabolic shift from oxidative phoshorylation to glycolysis is observed in somatic cells being reprogrammed to induced pluripotent stem cells (Sperber et al. 2015; Takashima et al. 2015). By generating a defined chemical environment, glycolysis also directs cells to adopt specific developmental fate decisions (Oginuma et al. 2020). In addition to energetic demands, proliferating adult stem cells have important metabolic requirements. Aerobic glycolysis fulfills some of these requirements by providing intermediates for biomass production and anabolic reactions (Lunt and Vander Heiden 2011). Here, we report that glycolysis-derived SBP is required for MuSC activation and proliferation of MuSC-derived myogenic progenitors. The essential function of Psat1 during development (White et al. 2013) has precluded its study in adult animals. Using $Pax7^{Cre}$ driver mouse lines, we have deleted Psat1 and observed that it is critical for MuSC biology. Pax7 is expressed in MuSCs, a subset of neurons, and cranofacial tissues (Buckingham and Relaix 2007). While the participation of non-MuSC Pax7^{+} cells in the observed muscle defects cannot be formally ruled out, cultured myoblasts isolated from $Psat1^{cKO}$ mice displayed proliferative defects, indicating a cell-autonomous function of Psat1. In addition to catalyzing the conversion of 3-phosphohydroxypyruvate (3PHP) to 3-phosphoserine, Psat1 generates α-KG using glutamate as a substrate. In a reverse reaction, α-KG generated by Psat1 accepts an amino group from the donor amino acid (transamination) to form glutamate, which is then converted to glutamine by glutamine synthetase. Selective and inducible genetic Psat1 ablation in MuSCs resulted in a lack of myogenic progenitor expansion and consequent impaired muscle regeneration following injury. Consistent with the observation that Psat1 was not appreciably expressed in quiescent MuSCs, $Psat1^{cKO}$ mice did not display obvious abnormalities in homeostatic conditions. Myogenic proliferation and muscle regeneration defects in $Psat1^{iKO}$ mice could be corrected by supplementation with either α-KG or glutamine. On the other hand, supplementation with serine-derived one-carbon folic acid or S-adenosyl methionine could not correct impaired proliferation of $Psat1^{cKO}$ myoblasts. α-KG or glutamine improved glycolysis in $Psat1^{cKO}$ myoblasts and in myoblasts derived from older mice. A direct role of α-KG on glutamine biosynthesis is suggested by increased intracellular glutamine levels that we observed after cell exposure to α-KG and reverse of the proliferative effect exerted by α-KG on $Psat1^{cKO}$ myoblasts upon pharmacological inhibition of glutamine synthethase. Serine and cysteine levels were not decreased in $Psat1^{cKO}$ myoblasts, a phenomenon likely explained by serine extracellular uptake (Yang and Vousden 2016). Normal levels of cysteine in $Psat1^{cKO}$ myoblasts might be explained by cystathioninase activity, which catalyzes the conversion of serine and homocysteine to cysteine and α-ketobutyrate (Stryer 1988). Overall, these findings point to a critical role of α-KG and glutamine in the proliferative defects observed in $Psat1^{cKO}$ myoblasts. With a Psat1-independent mechanism, macrophage-derived glutamine has been reported to boost MuSC activation and improve muscle regeneration through mTOR (Shang et al. 2020). However, it is unlikely that the positive effects of α-KG or glutamine that we have observed in MuSC proliferation and regeneration are mediated by mTOR activation. First, α-KG inhibits mTOR activity in Caenorhabditis elegans and mammalian cells (Chin et al. 2014). Second, mTOR activity is abnormally elevated in old mice, and its inhibition by rapalogs improves muscle regeneration and counteracts sarcopenia in aged animals (García-Prat et al. 2016; Joseph et al. 2019). α-KG maintains pluripotency of ESCs (Carey et al. 2015), and, through α-KG generation, Psat1 affects the timing of ESC differentiation by influencing ten-eleven translocation (TET) protein-mediated DNA 5′-hydroxymethylcytosine (5hmC) and histone methylation (Hwang et al. 2016). We have not observed significant changes of 5hmC or histone H3K27 or H3K9 methylation in $Psat1^{cKO}$ MuSCs, suggesting either cell type-specific effects or distinct α-KG stoichiometric requirements in regulating specific biological processes. Studies in humans have suggested the potential benefits of α-KG in muscle growth and wound healing and in promoting faster recovery after surgery (Cynober 1999, 2004; Donati et al. 1999). More recently, α-KG has been reported to extend life span in aging mice and to reduce biological age in humans (Asadi Shahmirzadi et al. 2020; Demidenko et al. 2021). In mice, α-KG was found to induce interleukin 10 (IL-10) expression and to suppress chronic inflammation (Asadi Shahmirzadi et al. 2020). In humans, α-KG plasma levels decline ∼10-fold between the ages of 40 and 80 yr old (Harrison and Pierzynowski 2008). Psat1, α-KG, and glutamine levels were all reduced in MuSCs isolated from aging mice, and IP injection of either α-KG or glutamine improved MuSC activation, promoted muscle regeneration, and reduced fibrosis of aged mice. Other metabolites, such as NAD^{+} precursors, improve muscle function in both aging rodents and humans (Ryu et al. 2016; Zhang et al. 2016; Pirinen et al. 2020). While a causative role of MuSCs in the pathogenesis of human sarcopenia remains to be firmly demonstrated, the number and regenerative potential of MuSCs are reduced during human aging

(Verdijk et al. 2014; Snijders et al. 2015). As there are no efficacious therapeutic interventions for sarcopenia (Cruz-Jentoft and Sayer 2019), α-KG or glutamine—alone or in various combinations with other metabolites, antioxidants (García-Prat et al. 2016), and rapalogs (Shavlakadze et al. 2018)—may constitute a potential pharmacological approach to improve MuSC function and muscle mass in the aging population.

Materials and methods

Animals

Mice were housed in a pathogen-free facility, and all experiments were performed according to the National Institutes of Health (NIH) Animal Care and Use regulations. $Psat1^{fl/fl}$ mice were generated at the Transgenic Core Facility of the National Heart, Lung, and Blood Institute (NHLBI) by CRISP/Cas9 insertion strategy. Guide RNAs, single-strand DNAs, and PCR primers for generating and genotyping the edited alleles are provided in Supplemental Table S4. The following mice were used: C57BL/6J (JAX 000664) and $Psat1^{fl/fl}$ crossed with either constitutive $Pax7^{Cre}$ ($Psat1^{cKO}$) (JAX 010530) (Keller et al. 2004) or tamoxifen-inducible $Pax7^{CreERT2}$ ($Psat1^{iKO}$) (JAX 017763). $Psat1^{iKO}$ mice were crossed with nuclear membrane-binding $ROSA26^{STOP-Sun-1-GFP}$ (JAX 021039) mice (Mo et al. 2015) to generate $Psat1^{iKO\ nGFP}$. $Psat1^{cKO}$, $Psat1^{iKO}$, and $Psat1^{iKO\ nGFP}$ mice and their respective control mice ($Pax7^{+/+};Psat1^{fl/fl}$, $Pax7^{CreERT2};Psat1^{+/+}$, and $Pax7^{CreERT2};Psat1^{+/+};ROSA26^{STOP-Sun-1-GFP}$) received 10 mg/mL tamoxifen (Sigma T5648) in corn oil via IP injection at 100 µL/d for five consecutive days. For comparative studies, age- and sex-matched littermates were used for all experimental procedures. Genotyping was done by a Taq-Man-based genotyping approach provided by Transnetyx, Inc. (http://www.transnetyx.com). Old (23–24-mo-old) and geriatric (32-mo-old) C57BL/6J mice were imported from Charles River Laboratories, Inc.

Mouse primary myoblast isolation and culture

Mouse primary myoblasts were isolated following the described methods (Liu et al. 2015; Riparini et al. 2022). Briefly, hindlimb muscles were dissociated into single cells by enzymatic digestion with 1000 U/mL collagenase II in Ham's F10 medium supplemented with 10% horse serum and 1% penicillin/streptomycin (wash medium [WM]) for 1 h at 37°C. Digested muscles were then subjected to further digestion with 1000 U/mL collagenase II and 11 U/mL dispase for 30 min. The cell suspension was then filtered and plated onto 10-cm plates and incubated overnight at 37°C and 5% CO_2. The following day, primary myoblasts were enriched by preplating. Primary myoblasts were cultured in WM supplemented with 2.5 ng/mL bFGF (control medium [CM]).

Human primary myoblasts

Human primary myoblasts were purchased from Cook MyoSite and culterd with MyoTonic basal medium (Cook MyoSite MB-2222) supplemented with MyoTonic growth supplement (Cook MyoSite MS-3333) and 1% penicillin/streptomycin. Human primary myoblasts were plated on at a density of 4×10^3 to 6×10^3 cells/cm^2.

Muscle injury

Mice were anesthetized in an isoflurane scavenging system with the appropriate pain relief measures (subcutaneous injection of 0.5 mL of 0.3 mg/mL buprenorphine for each mouse). Injury was induced by intramuscular injection of 50–100 µL of 2 µg/mL notexin (Accurate Chemical TXL8104-100) into the TA/EDL muscles with an insulin syringe. At the indicated times after injury, mice were euthanized and muscles were dissected for cryo-embedding or flow cytometry.

In vivo EdU labeling

$Psat1^{iKO\ nGFP}$ and their littermate control mice were injured by notexin injection and intraperitoneally injected with 100 µL of 25.5 mg/kg 5′-ethynyl-2′-deoxyuridine (EdU; Invitrogen A10044;) 1 h before being euthanized at 3 dpi. Muscles were collected and processed for immunofluorescence staining on tissue slides. EdU-labeled cells were detected using the Click-iT EdU imaging kit (Invitrogen C10086) following the manufacturer's protocol.

In vivo α-KG treatment

One-hundred microliters of 180 mg/mL KG (600 mg/kg body weight; Sigma 75890) or vehicle (1× PBS) was administered intraperitoneally to each mouse. Treatment was performed every other day for 7 d. TA/EDL muscles were collected at 3 or 28 dpi. For aged mice, injured muscles were collected at 15 or 28 dpi. TA/EDL muscles were cryo-embedded for further analysis.

In vivo glutamine treatment

Five-hundred microliters of 30 mg/mL L-glutamine (500 mg/kg body weight; Sigma G8580) or vehicle (1× PBS) was administered intraperitoneally. Treatment was performed every other day. Injured TA/EDL muscles were collected at either 3 or 28 dpi, cryo-embedded, and stored at −80°C for further analysis.

Ex vivo myoblast treatment

Primary myoblasts from 2- to 4-mo-old or aged (24- to 32-mo-old) control and $Psat1^{cKO}$ mice were cultured for one passage, and cells were plated at a density of 1.5×10^4 cells/cm^2 in CM. One day after plating, cells were treated for an additional 24 h with one of the following components: 1 mM DM-α-KG (Sigma T31458), 1 mM succinate (Sigma 73605), 4 mM glutamine (Gibco 25030-081), 4 mM glycine (MP Biomedicals 194681), 10 mM folic acid (Sigma F8758), or 10 µM SAM (Sigma A2408). EdU (10 µM) was supplied 2 h before cell harvesting. Cells were then fixed with 4% PFA for 10 min at room

temperature, washed three times for 5 min each with 1× PBS, and stored in 1× PBS at 4°C for the Click-iT EdU assay.

Muscle dissection, cryo-embedding, immunofluorescence, and Sirius red histology

The TA/EDL muscles obtained from uninjured or injured mice were processed at 3, 7, 15, and 28 dpi, respectively. The TA/EDL muscles were dissected, covered with OCT, snap-frozen in cold methylbutane, and stored at least overnight at −80°C before sectioning. Cryo-embedded tissues were mounted on a cryostat (Leica CM 1860) in the transverse direction and sectioned at 10-μm thickness. Sections were collected on Superfrost Plus slides (VWR 48311-703) and processed for immunofluorescence analysis. For immunofluorescence, $1 × 10^4$ myoblasts were plated on a collagen-coated 96-well plate. Myoblasts were fixed for 10 min with 2% PFA, permeabilized with 0.1% Triton/PBS, and further processed for immunofluorescence staining. Primary and secondary antibodies and their dilution ratios are listed in Supplemetal Table S4. Sirius red staining was performed using a kit (Abcam ab150681). Briefly, cryosections on slides were fixed with 4% PFA for 30 min and sequentially washed with 70%, 50%, and 30% ethanol and 1× PBS for 2 min for each step. Sections were stained in Sirius red solution for 10 min and then washed twice with acetic acid solution. Sections were further dehydrated with 100% ethanol and xylene and then mounted with Permount and cover slides.

Oxygen consumption and extracellular acidification analysis

Primary myoblasts were plated at $1.5 × 10^4$ cells/well in a collagen-coated 96-well Seahorse cell culture plate and cultured in CM. One day before measurements, 1 mM DM-α-KG was added to 1 mM medium for an additional 24 h. The XF calibrant (Agilent 100840) and a cartridge submerged in ddH$_2$O were maintained in a CO$_2$-free Seahorse incubator for 12 h. For the mitochondrial stress test, on the day of the Seahorse assay, CM was replaced with Seahorse assay medium (phenol red-free DMEM at pH 7.4, supplied with 25 mM glucose, 1 mM sodium pyruvate, 2 mM glutamine) and incubated in a CO$_2$-free Seahorse incubator for at least 45 min before the assay to deplete CO$_2$. Selected drugs were dissolved in Seahorse assay medium. Cells were treated serially with 1 μM oligomycin, 1 μM FCCP, and 2 μM rotenone-antimycin A, and oxygen consumption rates (OCR) were measured over time. For the glycolysis stress test, $1.5 × 10^4$ cells/well were plated onto a collagen-coated 96-well Seahorse plate in CM. One day after plating, cells were treated with 1 mM DM-α-KG, 4 mM glutamine (Gln), 1 mM MSO, or 4 mM MSO + DM-α-KG, MSO + Gln, or glycine (Gly) for an additional 24 h. On the day of the experiment, CM was replaced with Seahorse assay medium (phenol red-free DMEM at pH 7.4, supplied with 2 mM glutamine). Cells were treated serially with 25 mM glucose, 1 μM oligomycin, and 100 mM 2-DG, and the extracellular acidifi-

cation rate (ECAR) was measured over time. Statistical analysis relative to Supplemental Figure S4, E and G, was performed using the same control group (Ctrl_CM or *Psat1*^{cKO}_CM).

Metabolomics

Isolated primary myoblasts were plated onto a 10-cm collagen-coated dish for 24 h and transfected with scrambled siRNA control or siRNA targeting the *Psat1* gene and then collected 48 h after silencing. Briefly, cells were trypsinized, washed twice in 1× PBS, snap-frozen in liquid nitrogen, and then stored at −80°C until analysis. Untargeted metabolomics was performed at West Coast Metabolomics (University of California, Davis) for the following group of metabolites: carbohydrates, sugar phosphate, amino acids, hydroxyl acids, free fatty acids, purines, pyrimidines, aromatics, and exposome-derived chemicals. A full list of the metabolites screened is available as primary metabolism analysis at https://metabolomics.ucdavis.edu/core-services/metabolites. Briefly, samples were extracted using the Matyash extraction procedure, which includes MTBE, MeOH, and H$_2$O. The aqueous (bottom) phase was dried and subjected to derivatization for gas chromatography (GC). Analysis was performed on an Agilent 7890 GC (Agilent) coupled with a Leco Pegasus IV TOF (Leco). Using a splitless method, 0.5 μL of derivatized sample was injected onto a Restek RTX-5SIL (Restek Bellefonte 12723-127) MS column with an Integra-Guard at 275°C with a helium flow of 1 mL/min. The transfer line was set to 280°C, and the EI ion source was set to 250°C. The mass spectrometry parameters of collected data are from 85 to 500 m/z at an acquisition rate of 17 spectra/sec.

Metabolomic analysis

Univariate analyses were performed as described (Chen et al. 2022). Metabolite differences between the two groups (si-Psat1 vs. si-Ctrl myoblasts) were identified by Welch's independent sample t-tests, with the peak height of each metabolite as the dependent variable. Significantly changed metabolites were selected based on P-value ≤ 0.05.

α-KG measurements

Primary myoblasts ($1 × 10^6$) were counted using an automated cytometer (Cellometer Vision, Nexcelom) and immediately processed for α-KG assay (Abcam ab83431) following the manufacturer's instructions. α-KG values were normalized to total protein levels.

Glutamine/glutamate assays

Control, *Psat1*^{cKO}, or aged myoblasts ($1 × 10^4$ per well) were plated onto a collagen-coated 96-well plate. The following day, cells were treated with 1 mM DM-α-KG for an additional 24 h. Cells were incubated for 5 min with 15 mL of inactivation solution (0.3 N HCl; Mallinckrodt Baker UN1789), followed by 1-min incubation with Tris

solution (450 mM Tris at pH 8.5; SAFC RES9680T-A102X). For each sample, 25-µL aliquots were transferred into two wells of a 96-well white luminometer plate (Greiner 655075). These wells were used to determine the signal of glutamine plus glutamate and of glutamate only, following the manufacturer's protocol (Promega J8021). To evaluate glutamine levels, the signal from glutamate-only wells was subtracted from that of the total glutamine plus glutamate wells. The signal was normalized on cell viability.

RNA-seq

For RNA-seq, Illumina RNA libraries were prepared with an NEBNext Ultra II RNA library preparation kit for Illumina (NEB E7490) according to the manufacturer's instructions. Briefly, 250 ng of total RNA from Ctrl or $Psat1^{iKO}$ 3-dpi MuSCs or 500 ng of total RNA from Ctrl or $Psat1^{cKO}$ myoblasts was enriched for poly(A)$^+$ mRNA and retrotranscribed. cDNA was then fragmented and adapters were added to both ends of the fragments. The obtained libraries were amplified and size-selected before NGS. All libraries were diluted to 3 nM and sequenced on an Illumina NovaSeq6000 or Illumina NextSeq550 using the following read length: 50 bp for read1, 8 bp for the I7 index, and 50 bp for read2.

RNA-seq analysis

For 3-dpi Ctrl or $Psat1^{iKO}$ analysis, paired-end reads were aligned to the mm10 reference genome using HISAT2 version 2.2.1 (Kim et al. 2019) and default parameters. Aligned reads were quantified using Sailfish (Patro et al. 2014) and annotated in R using the org.Mm.eg.db package version 3.15.0. Differential expression analysis was performed using DESeq2 pipeline version 4.2.0 (Love et al. 2014). Genes with a fold change of Ctrl/$Psat1^{iKO}$ >2 and adjusted P-value of <0.05 were selected as significantly differentially expressed. For Ctrl and $Psat1^{cKO}$ myoblast analysis, the FastQ files were produced by processing raw sequencing data using bcl2fastq (v2.20.0). Subsequently, sequence reads were aligned to the mouse genome build mm10 using TopHat 2.1.1. Gene expression values, measured in reads per kilobase per million mapped reads (RPKM), were computed using Partek Genomic suite 7.21.119. Differential gene expression analysis was conducted through ANOVA (Partek Genomic suite), applying fold change criteria of 1.5 and a significance cutoff of $P < 0.05$. Sequencing data sets have been deposited in the GEO repository under accession number GSE248916.

Statistical analysis

All of the experiments were conducted with at least three biological replicates. Sample size for each experiment is shown in the figures and legends. Statistical significance was determined using two-tailed Student's t-test (unpaired for unrelated samples and paired for biologically matched samples; GraphPad software 10.0). Quantitative data displayed as histograms are expressed as mean ± SEM

unless otherwise indicated. Sequencing data analysis parameters are described in the Supplemental Material.

References

Agathocleous M, Love NK, Randlett O, Harris JJ, Liu J, Murray AJ, Harris WA. 2012. Metabolic differentiation in the embryonic retina. *Nat Cell Biol* **14:** 859–864. doi:10.1038/ncb2531

Almada AE, Wagers AJ. 2016. Molecular circuitry of stem cell fate in skeletal muscle regeneration, ageing and disease. *Nat Rev Mol Cell Biol* **17:** 267–279. doi:10.1038/nrm.2016.7

Asadi Shahmirzadi A, Edgar D, Liao CY, Hsu YM, Lucanic M, Asadi Shahmirzadi A, Wiley CD, Gan G, Kim DE, Kasler HG, et al. 2020. α-Ketoglutarate, an endogenous metabolite, extends lifespan and compresses morbidity in aging mice. *Cell Metab* **32:** 447–456.e6. doi:10.1016/j.cmet.2020.08.004

Baker N, Wade S, Triolo M, Girgis J, Chwastek D, Larrigan S, Feige P, Fujita R, Crist C, Rudnicki MA, et al. 2022. The mitochondrial protein OPA1 regulates the quiescent state of adult muscle stem cells. *Cell Stem Cell* **29:** 1315–1332.e9. doi:10.1016/j.stem.2022.07.010

Baraibar MA, Hyzewicz J, Rogowska-Wrzesinska A, Bulteau AL, Prip-Buus C, Butler-Browne G, Friguet B. 2016. Impaired energy metabolism of senescent muscle satellite cells is associated with oxidative modifications of glycolytic enzymes. *Aging (Albany NY)* **8:** 3375–3389. doi:10.18632/aging.101126

Bernet JD, Doles JD, Hall JK, Kelly Tanaka K, Carter TA, Olwin BB. 2014. P38 MAPK signaling underlies a cell-autonomous loss of stem cell self-renewal in skeletal muscle of aged mice. *Nat Med* **20:** 265–271. doi:10.1038/nm.3465

Brack AS, Conboy MJ, Roy S, Lee M, Kuo CJ, Keller C, Rando TA. 2007. Increased Wnt signaling during aging alters muscle stem cell fate and increases fibrosis. *Science* **317:** 807–810. doi:10.1126/science.1144090

Buckingham M, Relaix F. 2007. The role of *Pax* genes in the development of tissues and organs: *Pax3* and *Pax7* regulate muscle progenitor cell functions. *Annu Rev Cell Dev Biol* **23:** 645–673. doi:10.1146/annurev.cellbio.23.090506.123438

Carey BW, Finley LW, Cross JR, Allis CD, Thompson CB. 2015. Intracellular α-ketoglutarate maintains the pluripotency of embryonic stem cells. *Nature* **518:** 413–416. doi:10.1038/nature13981

Carlson ME, Suetta C, Conboy MJ, Aagaard P, Mackey A, Kjaer M, Conboy I. 2009. Molecular aging and rejuvenation of human muscle stem cells. *EMBO Mol Med* **1:** 381–391. doi:10.1002/emmm.200900045

Cerletti M, Jang YC, Finley LW, Haigis MC, Wagers AJ. 2012. Short-term calorie restriction enhances skeletal muscle stem cell function. *Cell Stem Cell* **10:** 515–519. doi:10.1016/j.stem.2012.04.002

Chakkalakal JV, Jones KM, Basson MA, Brack AS. 2012. The aged niche disrupts muscle stem cell quiescence. *Nature* **490:** 355–360. doi:10.1038/nature11438

Chen Y, Li EM, Xu LY. 2022. Guide to metabolomics analysis: a Bioinformatics workflow. *Metabolites* **12:** 357. doi:10.3390/metabo12040357

Chin RM, Fu X, Pai MY, Vergnes L, Hwang H, Deng G, Diep S, Lomenick B, Meli VS, Monsalve GC, et al. 2014. The metabolite α-ketoglutarate extends lifespan by inhibiting ATP synthase and TOR. *Nature* **510:** 397–401. doi:10.1038/nature13264

Conboy IM, Conboy MJ, Smythe GM, Rando TA. 2003. Notch-mediated restoration of regenerative potential to aged muscle. *Science* **302:** 1575–1577. doi:10.1126/science.1087573

Cosgrove BD, Gilbert PM, Porpiglia E, Mourkioti F, Lee SP, Corbel SY, Llewellyn ME, Delp SL, Blau HM. 2014. Rejuvenation of the muscle stem cell population restores strength to injured aged muscles. *Nat Med* **20:** 255–264. doi:10.1038/nm.3464

Cruz-Jentoft AJ, Sayer AA. 2019. Sarcopenia. *Lancet* **393:** 2636–2646. doi:10.1016/S0140-6736(19)31138-9

Cynober LA. 1999. The use of α-ketoglutarate salts in clinical nutrition and metabolic care. *Curr Opin Clin Nutr Metab Care* **2:** 33–37. doi:10.1097/00075197-199901000-00007

Cynober L. 2004. Ornithine α-ketoglutarate as a potent precursor of arginine and nitric oxide: a new job for an old friend. *J Nutr* **134:** 2858S–2862S; discussion 2895S. doi:10.1093/jn/134.10.2858S

Das S, Morvan F, Morozzi G, Jourde B, Minetti GC, Kahle P, Rivet H, Brebbia P, Toussaint G, Glass DJ, et al. 2017. ATP citrate lyase regulates myofiber differentiation and increases regeneration by altering histone acetylation. *Cell Rep* **21:** 3003–3011. doi:10.1016/j.celrep.2017.11.038

Dell'Orso S, Juan AH, Ko KD, Naz F, Perovanovic J, Gutierrez-Cruz G, Feng X, Sartorelli V. 2019. Single cell analysis of adult mouse skeletal muscle stem cells in homeostatic and regenerative conditions. *Development* **146:** dev174177. doi:10.1242/dev.174177

Demidenko O, Barardo D, Budovskii V, Finnemore R, Palmer FR, Kennedy BK, Budovskaya YV. 2021. Rejuvant, a potential life-extending compound formulation with α-ketoglutarate and vitamins, conferred an average 8 year reduction in biological aging, after an average of 7 months of use, in the TruAge DNA methylation test. *Aging* **13:** 24485–24499. doi:10.18632/aging.203736

Donati L, Ziegler F, Pongelli G, Signorini MS. 1999. Nutritional and clinical efficacy of ornithine α-ketoglutarate in severe burn patients. *Clin Nutr* **18:** 307–311. doi:10.1016/S0261-5614(98)80029-0

Dong A, Liu J, Lin K, Zeng W, So WK, Hu S, Cheung TH. 2022. Global chromatin accessibility profiling analysis reveals a chronic activation state in aged muscle stem cells. *iScience* **25:** 104954. doi:10.1016/j.isci.2022.104954

Englund DA, Murach KA, Dungan CM, Figueiredo VC, Vechetti IJ Jr, Dupont-Versteegden EE, McCarthy JJ, Peterson CA. 2020. Depletion of resident muscle stem cells negatively impacts running volume, physical function, and muscle fiber hypertrophy in response to lifelong physical activity. *Am J Physiol Cell Physiol* **318:** C1178–C1188. doi:10.1152/ajpcell.00090.2020

Evano B, Khalilian S, Le Carrou G, Almouzni G, Tajbakhsh S. 2020. Dynamics of asymmetric and symmetric divisions of muscle stem cells in vivo and on artificial niches. *Cell Rep* **30:** 3195–3206.e7. doi:10.1016/j.celrep.2020.01.097

Feige P, Brun CE, Ritso M, Rudnicki MA. 2018. Orienting muscle stem cells for regeneration in homeostasis, aging, and disease. *Cell Stem Cell* **23:** 653–664. doi:10.1016/j.stem.2018.10.006

Fry CS, Lee JD, Mula J, Kirby TJ, Jackson JR, Liu F, Yang L, Mendias CL, Dupont-Versteegden EE, McCarthy JJ, et al. 2015. Inducible depletion of satellite cells in adult, sedentary mice impairs muscle regenerative capacity without affecting sarcopenia. *Nat Med* **21:** 76–80. doi:10.1038/nm.3710

García-Prat L, Martinez-Vicente M, Perdiguero E, Ortet L, Rodríguez-Ubreva J, Rebollo E, Ruiz-Bonilla V, Gutarra S, Ballestar E, Serrano AL, et al. 2016. Autophagy maintains stemness by preventing senescence. *Nature* **529:** 37–42. doi:10.1038/nature16187

García-Prat L, Sousa-Victor P, Muñoz-Cánoves P. 2017. Proteostatic and metabolic control of stemness. *Cell Stem Cell* **20:** 593–608. doi:10.1016/j.stem.2017.04.011

Gheller BJ, Blum JE, Lim EW, Handzlik MK, Hannah Fong EH, Ko AC, Khanna S, Gheller ME, Bender EL, Alexander MS, et al. 2021. Extracellular serine and glycine are required for mouse and human skeletal muscle stem and progenitor cell function. *Mol Metab* **43:** 101106. doi:10.1016/j.molmet.2020.101106

Harrison AP, Pierzynowski SG. 2008. Biological effects of 2-oxoglutarate with particular emphasis on the regulation of protein, mineral and lipid absorption/metabolism, muscle performance, kidney function, bone formation and cancerogenesis, all viewed from a healthy ageing perspective state of the art--review article. *J Physiol Pharmacol* **59:** 91–106.

Hong X, Isern J, Campanario S, Perdiguero E, Ramírez-Pardo I, Segalés J, Hernansanz-Agustín P, Curtabbi A, Deryagin O, Pollán A, et al. 2022. Mitochondrial dynamics maintain muscle stem cell regenerative competence throughout adult life by regulating metabolism and mitophagy. *Cell Stem Cell* **29:** 1506–1508. doi:10.1016/j.stem.2022.09.002

Hwang IY, Kwak S, Lee S, Kim H, Lee SE, Kim JH, Kim YA, Jeon YK, Chung DH, Jin X, et al. 2016. Psat1-dependent fluctuations in α-ketoglutarate affect the timing of ESC differentiation. *Cell Metab* **24:** 494–501. doi:10.1016/j.cmet.2016.06.014

Islam MS, Leissing TM, Chowdhury R, Hopkinson RJ, Schofield CJ. 2018. 2-oxoglutarate-dependent oxygenases. *Annu Rev Biochem* **87:** 585–620. doi:10.1146/annurev-biochem-061516-044724

Jones RG, Thompson CB. 2007. Revving the engine: signal transduction fuels T cell activation. *Immunity* **27:** 173–178. doi:10.1016/j.immuni.2007.07.008

Joseph GA, Wang SX, Jacobs CE, Zhou W, Kimble GC, Tse HW, Eash JK, Shavlakadze T, Glass DJ. 2019. Partial inhibition of mTORC1 in aged rats counteracts the decline in muscle mass and reverses molecular signaling associated with sarcopenia. *Mol Cell Biol* **39:** e00141-19. doi:10.1128/MCB.00141-19

Kann AP, Hung M, Wang W, Nguyen J, Gilbert PM, Wu Z, Krauss RS. 2022. An injury-responsive Rac-to-Rho GTPase switch drives activation of muscle stem cells through rapid

cytoskeletal remodeling. *Cell Stem Cell* **29:** 933–947.e6. doi:10.1016/j.stem.2022.04.016

Keller C, Hansen MS, Coffin CM, Capecchi MR. 2004. *Pax3:Fkhr* interferes with embryonic *Pax3* and *Pax7* function: implications for alveolar rhabdomyosarcoma cell of origin. *Genes Dev* **18:** 2608–2613. doi:10.1101/gad.1243904

Kim D, Paggi JM, Park C, Bennett C, Salzberg SL. 2019. Graph-based genome alignment and genotyping with HISAT2 and HISAT-genotype. *Nat Biotechnol* **37:** 907–915. doi:10.1038/s41587-019-0201-4

Klose RJ, Zhang Y. 2007. Regulation of histone methylation by demethylimination and demethylation. *Nat Rev Mol Cell Biol* **8:** 307–318. doi:10.1038/nrm2143

Krajewski WW, Collins R, Holmberg-Schiavone L, Jones TA, Karlberg T, Mowbray SL. 2008. Crystal structures of mammalian glutamine synthetases illustrate substrate-induced conformational changes and provide opportunities for drug and herbicide design. *J Mol Biol* **375:** 217–228. doi:10.1016/j.jmb.2007.10.029

Krawczyk CM, Holowka T, Sun J, Blagih J, Amiel E, DeBerardinis RJ, Cross JR, Jung E, Thompson CB, Jones RG, et al. 2010. Toll-like receptor-induced changes in glycolytic metabolism regulate dendritic cell activation. *Blood* **115:** 4742–4749. doi:10.1182/blood-2009-10-249540

Kuang S, Kuroda K, Le Grand F, Rudnicki MA. 2007. Asymmetric self-renewal and commitment of satellite stem cells in muscle. *Cell* **129:** 999–1010. doi:10.1016/j.cell.2007.03.044

Liu L, Cheung TH, Charville GW, Rando TA. 2015. Isolation of skeletal muscle stem cells by fluorescence-activated cell sorting. *Nat Protoc* **10:** 1612–1624. doi:10.1038/nprot.2015.110

Liu L, Charville GW, Cheung TH, Yoo B, Santos PJ, Schroeder M, Rando TA. 2018. Impaired notch signaling leads to a decrease in p53 activity and mitotic catastrophe in aged muscle stem cells. *Cell Stem Cell* **23:** 544–556.e4. doi:10.1016/j.stem.2018.08.019

Locasale JW, Cantley LC. 2011. Metabolic flux and the regulation of mammalian cell growth. *Cell Metab* **14:** 443–451. doi:10.1016/j.cmet.2011.07.014

Love MI, Huber W, Anders S. 2014. Moderated estimation of fold change and dispersion for RNA-seq data with DESeq2. *Genome Biol* **15:** 550. doi:10.1186/s13059-014-0550-8

Lukjanenko L, Karaz S, Stuelsatz P, Gurriaran-Rodriguez U, Michaud J, Dammone G, Sizzano F, Mashinchian O, Ancel S, Migliavacca E, et al. 2019. Aging disrupts muscle stem cell function by impairing matricellular WISP1 secretion from fibro-adipogenic progenitors. *Cell Stem Cell* **24:** 433–446.e7. doi:10.1016/j.stem.2018.12.014

Lunt SY, Vander Heiden MG. 2011. Aerobic glycolysis: meeting the metabolic requirements of cell proliferation. *Annu Rev Cell Dev Biol* **27:** 441–464. doi:10.1146/annurev-cellbio-092910-154237

Ma N, Chen D, Lee JH, Kuri P, Hernandez EB, Kocan J, Mahmood H, Tichy ED, Rompolas P, Mourkioti F. 2022. Piezo1 regulates the regenerative capacity of skeletal muscles via orchestration of stem cell morphological states. *Sci Adv* **8:** eabn0485. doi:10.1126/sciadv.abn0485

Machado L, Esteves de Lima J, Fabre O, Proux C, Legendre R, Szegedi A, Varet H, Ingerslev LR, Barrès R, Relaix F, et al. 2017. In situ fixation redefines quiescence and early activation of skeletal muscle stem cells. *Cell Rep* **21:** 1982–1993. doi:10.1016/j.celrep.2017.10.080

Mo A, Mukamel EA, Davis FP, Luo C, Henry GL, Picard S, Urich MA, Nery JR, Sejnowski TJ, Lister R, et al. 2015. Epigenomic signatures of neuronal diversity in the mammalian brain. *Neuron* **86:** 1369–1384. doi:10.1016/j.neuron.2015.05.018

Moiseeva V, Cisneros A, Sica V, Deryagin O, Lai Y, Jung S, Andrés E, An J, Segalés J, Ortet L, et al. 2023. Senescence atlas reveals an aged-like inflamed niche that blunts muscle regeneration. *Nature* **613:** 169–178. doi:10.1038/s41586-022-05535-x

Oginuma M, Harima Y, Tarazona OA, Diaz-Cuadros M, Michaut A, Ishitani T, Xiong F, Pourquié O. 2020. Intracellular pH controls WNT downstream of glycolysis in amniote embryos. *Nature* **584:** 98–101. doi:10.1038/s41586-020-2428-0

Pala F, Di Girolamo D, Mella S, Yennek S, Chatre L, Ricchetti M, Tajbakhsh S. 2018. Distinct metabolic states govern skeletal muscle stem cell fates during prenatal and postnatal myogenesis. *J Cell Sci* **131.** doi:10.1242/jcs.212977

Palla AR, Ravichandran M, Wang YX, Alexandrova L, Yang AV, Kraft P, Holbrook CA, Schürch CM, Ho ATV, Blau HM. 2021. Inhibition of prostaglandin-degrading enzyme 15-PGDH rejuvenates aged muscle mass and strength. *Science* **371:** eabc8059. doi:10.1126/science.abc8059

Patro R, Mount SM, Kingsford C. 2014. Sailfish enables alignment-free isoform quantification from RNA-seq reads using lightweight algorithms. *Nat Biotechnol* **32:** 462–464. doi:10.1038/nbt.2862

Pirinen E, Auranen M, Khan NA, Brilhante V, Urho N, Pessia A, Hakkarainen A, Ulla Heinonen JK, Schmidt MS, Haimilahti K, et al. 2020. Niacin cures systemic NAD$^+$ deficiency and improves muscle performance in adult-onset mitochondrial myopathy. *Cell Metab* **32:** 144. doi:10.1016/j.cmet.2020.05.020

Relaix F, Bencze M, Borok MJ, Der Vartanian A, Gattazzo F, Mademtzoglou D, Perez-Diaz S, Prola A, Reyes-Fernandez PC, Rotini A, et al. 2021. Perspectives on skeletal muscle stem cells. *Nat Commun* **12:** 692. doi:10.1038/s41467-020-20760-6

Riparini G, Simone JM, Sartorelli V. 2022. FACS-isolation and culture of fibro-adipogenic progenitors and muscle stem cells from unperturbed and injured mouse skeletal muscle. *J Vis Exp* doi:10.3791/63983

Rodgers JT, King KY, Brett JO, Cromie MJ, Charville GW, Maguire KK, Brunson C, Mastey N, Liu L, Tsai CR, et al. 2014. mTORC1 controls the adaptive transition of quiescent stem cells from G_0 to g_{Alert}. *Nature* **510:** 393–396. doi:10.1038/nature13255

Ryall JG, Cliff T, Dalton S, Sartorelli V. 2015a. Metabolic reprogramming of stem cell epigenetics. *Cell Stem Cell* **17:** 651–662. doi:10.1016/j.stem.2015.11.012

Ryall JG, Dell'Orso S, Derfoul A, Juan A, Zare H, Feng X, Clermont D, Koulnis M, Gutierrez-Cruz G, Fulco M, et al. 2015b. The NAD$^+$-dependent SIRT1 deacetylase translates a metabolic switch into regulatory epigenetics in skeletal muscle stem cells. *Cell Stem Cell* **16:** 171–183. doi:10.1016/j.stem.2014.12.004

Ryu D, Zhang H, Ropelle ER, Sorrentino V, Mazala DA, Mouchiroud L, Marshall PL, Campbell MD, Ali AS, Knowels GM, et al. 2016. NAD$^+$ repletion improves muscle function in muscular dystrophy and counters global PARylation. *Sci Transl Med* **8:** 361ra139. doi:10.1126/scitranslmed.aaf5504

Shang M, Cappellesso F, Amorim R, Serneels J, Virga F, Eelen G, Carobbio S, Rincon MY, Maechler P, De Bock K, et al. 2020. Macrophage-derived glutamine boosts satellite cells and muscle regeneration. *Nature* **587:** 626–631. doi:10.1038/s41586-020-2857-9

Shavlakadze T, Zhu J, Wang S, Zhou W, Morin B, Egerman MA, Fan L, Wang Y, Iartchouk O, Meyer A, et al. 2018. Short-term low-dose mTORC1 inhibition in aged rats counter-regulates age-related gene changes and blocks age-related kidney pathology. *J Gerontol A Biol Sci Med Sci* **73:** 845–852. doi:10.1093/gerona/glx249

Shavlakadze T, Xiong K, Mishra S, McEwen C, Gadi A, Wakai M, Salmon H, Stec MJ, Negron N, Ni M, et al. 2023. Age-related gene expression signatures from limb skeletal muscles and the diaphragm in mice and rats reveal common and species-specific changes. *Skelet Muscle* **13:** 11. doi:10.1186/s13395-023-00321-3

Snijders T, Nederveen JP, McKay BR, Joanisse S, Verdijk LB, van Loon LJ, Parise G. 2015. Satellite cells in human skeletal muscle plasticity. *Front Physiol* **6:** 283. doi:10.3389/fphys.2015.00283

Sousa-Victor P, García-Prat L, Munoz-Canoves P. 2022. Control of satellite cell function in muscle regeneration and its disruption in ageing. *Nat Rev Mol Cell Biol* **23:** 204–226. doi:10.1038/s41580-021-00421-2

Sperber H, Mathieu J, Wang Y, Ferreccio A, Hesson J, Xu Z, Fischer KA, Devi A, Detraux D, Gu H, et al. 2015. The metabolome regulates the epigenetic landscape during naive-to-primed human embryonic stem cell transition. *Nat Cell Biol* **17:** 1523–1535. doi:10.1038/ncb3264

Stryer L. 1988. *Biochemistry*. W.H. Freeman and Company, New York.

Takashima Y, Guo G, Loos R, Nichols J, Ficz G, Krueger F, Oxley D, Santos F, Clarke J, Mansfield W, et al. 2015. Resetting transcription factor control circuitry toward ground-state pluripotency in human. *Cell* **162:** 452–453. doi:10.1016/j.cell.2015.06.052

Tang AH, Rando TA. 2014. Induction of autophagy supports the bioenergetic demands of quiescent muscle stem cell activation. *EMBO J* **33:** 2782–2797. doi:10.15252/embj.201488278

Tran TQ, Hanse EA, Habowski AN, Li H, Ishak Gabra MB, Yang Y, Lowman XH, Ooi AM, Liao SY, Edwards RA, et al. 2020. α-Ketoglutarate attenuates Wnt signaling and drives differentiation in colorectal cancer. *Nat Cancer* **1:** 345–358. doi:10.1038/s43018-020-0035-5

Verdijk LB, Snijders T, Drost M, Delhaas T, Kadi F, van Loon LJ. 2014. Satellite cells in human skeletal muscle; from birth to old age. *Age (Dordr)* **36:** 545–557. doi:10.1007/s11357-013-9583-2

Wang Z, Wei D, Bin E, Li J, Jiang K, Lv T, Mao X, Wang F, Dai H, Tang N. 2023. Enhanced glycolysis-mediated energy production in alveolar stem cells is required for alveolar regeneration. *Cell Stem Cell* **30:** 1028–1042.e7. doi:10.1016/j.stem.2023.07.007

White JK, Gerdin AK, Karp NA, Ryder E, Buljan M, Bussell JN, Salisbury J, Clare S, Ingham NJ, Podrini C, et al. 2013. Genome-wide generation and systematic phenotyping of knockout mice reveals new roles for many genes. *Cell* **154:** 452–464. doi:10.1016/j.cell.2013.06.022

Yang M, Vousden KH. 2016. Serine and one-carbon metabolism in cancer. *Nat Rev Cancer* **16:** 650–662. doi:10.1038/nrc.2016.81

Yin H, Price F, Rudnicki MA. 2013. Satellite cells and the muscle stem cell niche. *Physiol Rev* **93:** 23–67. doi:10.1152/physrev.00043.2011

Yucel N, Wang YX, Mai T, Porpiglia E, Lund PJ, Markov G, Garcia BA, Bendall SC, Angelo M, Blau HM. 2019. Glucose metabolism drives histone acetylation landscape transitions that dictate muscle stem cell function. *Cell Rep* **27:** 3939–3955.e6. doi:10.1016/j.celrep.2019.05.092

Zeng W, Yue L, Lam KSW, Zhang W, So WK, Tse EHY, Cheung TH. 2022. CPEB1 directs muscle stem cell activation by reprogramming the translational landscape. *Nat Commun* **13:** 947. doi:10.1038/s41467-022-28612-1

Zhang H, Ryu D, Wu Y, Gariani K, Wang X, Luan P, D'Amico D, Ropelle ER, Lutolf MP, Aebersold R, et al. 2016. NAD⁺ repletion improves mitochondrial and stem cell function and enhances life span in mice. *Science* **352:** 1436–1443. doi:10.1126/science.aaf2693